Synthesis of Functionalized Few Layer Graphene *via* Electrochemical Expansion

by

Intak Jeon

Master of Engineering, Korea University (2011)

Bachelor of Science, Korea University (2009)

Submitted to the Department of Materials Science and Engineering

in partial fulfillment of the requirements for the degree of

Master of Science in Materials Science and Engineering

at the

MASSACHUSETTS INSTITUTE OF TECHNOLOGY

February 2015

Author…….

Intak Jeon

Department of Materials Science and Engineering

October 23, 2014

Certified by ……...

Timothy M. Swager

John D. MacArthur Professor of Department of Chemistry

Thesis Supervisor

Certified by ……...

Michael F. Rubner

TDK Professor of Department of Materials Science and Engineering

Thesis reader

Accepted by……..

Donald R. Sadoway

John F. Elliott Professor of Materials Chemistry

Chairman, Departmental Committee on Graduate Students

Synthesis of Functionalized Few Layer Graphene *via* Electrochemical Expansion

by

Intak Jeon

Submitted to the Department of Materials Science and Engineering
on October 23, 2014 in partial fulfillment of the requirements for the degree of
Master of Science in Materials Science and Engineering

Abstract

Single layer graphene is a nearly transparent two-dimensional honeycomb sp^2 hybridized carbon lattice, and has received immense attention for its potential application in next-generation electronic devices, composite materials, and energy storage devices. This attention is a result of its desirable and intriguing electrical, mechanical, and chemical properties. However, mass production of high-quality, solution-processable graphene via a simple low-cost method remains a major challenge. Recently, electrochemical exfoliation of graphite has attracted attention as an easy, fast, and environmentally friendly approach to the production of high-quality graphene. This route solution phase approach complements the original micromechanical cleavage production of high quality graphite samples and also involved a chemically activated intermediate state that facilitates functionalization. In this thesis we demonstrate a highly efficient electrochemical exfoliation of graphite in organic solvent containing tetraalkylammonium salts, avoiding oxidation of graphene and the associated defect generation encountered with the broadly used Hummer's method. The expansion and charging of the graphite by intercalation of cations facilitates the functionalization of the graphene basal surfaces. Electrochemically enhanced diazonium functionalization of the expanded graphite was performed. The exfoliated graphene platelets were analyzed by Raman spectroscopy, to quantify defect states and the degree of exfoliation. Additional microscopy techniques provided additional insight into the chemical state and structure of the graphene sheets.

Thesis Supervisor: Timothy M. Swager
Title: John D. MacArthur Professor of Chemistry

Acknowledgements

Firstly, I would like to thank my advisor Prof. Timothy M. Swager for his advisement, encouragement and guidance during the course of this research as well as going out of his way to help me succeed and pursue my goals during my challenging time at MIT and also the freedom he provided while conducting research and his valuable opinions and insights, allowed me to expand my ideas and move in the right direction, promoting scientific growth and maturity. I would also like to extend my gratitude to Professor Michael Rubner, my thesis reader.

To all the present members of the Swager group, it has been an immense pleasure and privilege working with everyone and being part of such a diverse and intelligent group of talented individuals. In particular, I would like to express my gratitude to colleagues whom I have worked very closely with during the completion of this research: Lionel Moh, Dr. Katsuaki Kawasumi sensei, Dr. Carlos Zuniga, Dr. Bora Yoon, Byung Jin, Grace Han, Dr. Tsuyoshi Goya, John Goods, and Tran Ngoc Bao Truong for helping in the execution of several experiments as well as all their help in teaching me many experimental and analytical methods in the lab, and their input, advice and feedback on my work.

Last but not least, I would like to acknowledge, from the bottom of my heart all of my DMSE friends, KGSA family, KGSA soccer team, in no particular order, who provided a nice environment during this past 2 years: we shared many discussion, problems set, soccer games, meals, movies etc. I am appreciative the unconditional friendship that made us closer each and every day.

I would like to thank Jungsung culture foundation and Saudi Aramco for funding. I appreciate the help I received from the management and staff members at MIT-DMSE, and the Institute for Soldier Nanotechnology (ISN). Thank you.

Table of Contents

List of figures

List of tables

Chapter 1.

Introduction

1.1 The New Revolutionary and Disruptive 2-D Graphene

Graphene is a two-dimensional (2-D) atomic crystal that has unique properties. As opposed to other carbon materials (i.e. 3-D diamond and graphite, 1-D carbon nanotubes, and 0-D C_{60} molecule) graphene is a perfect 2-D lattice as shown in Figure 1. Graphene displays a number of interesting material properties including high strength (intrinsic strength of 130 GPa) and elasticity (Young's modulus of 1 TPa), very high electron mobility (2.5×10^5 $cm^2V^{-1}s^{-1}$), high thermal conductivity (> 3,000~5000 WmK^{-1}), and low optical absorption coefficient (2.3%). [1-5] Graphene can also be chemically functionalized to create a range of advanced materials. [6] Since its discovery graphene research has expanded at a fast pace and it is clear that this material is of tremendous importance to future technology. Key opportunities are likely to be based on technologies such as printable and flexible electronics, solar cells, and supercapacitors.

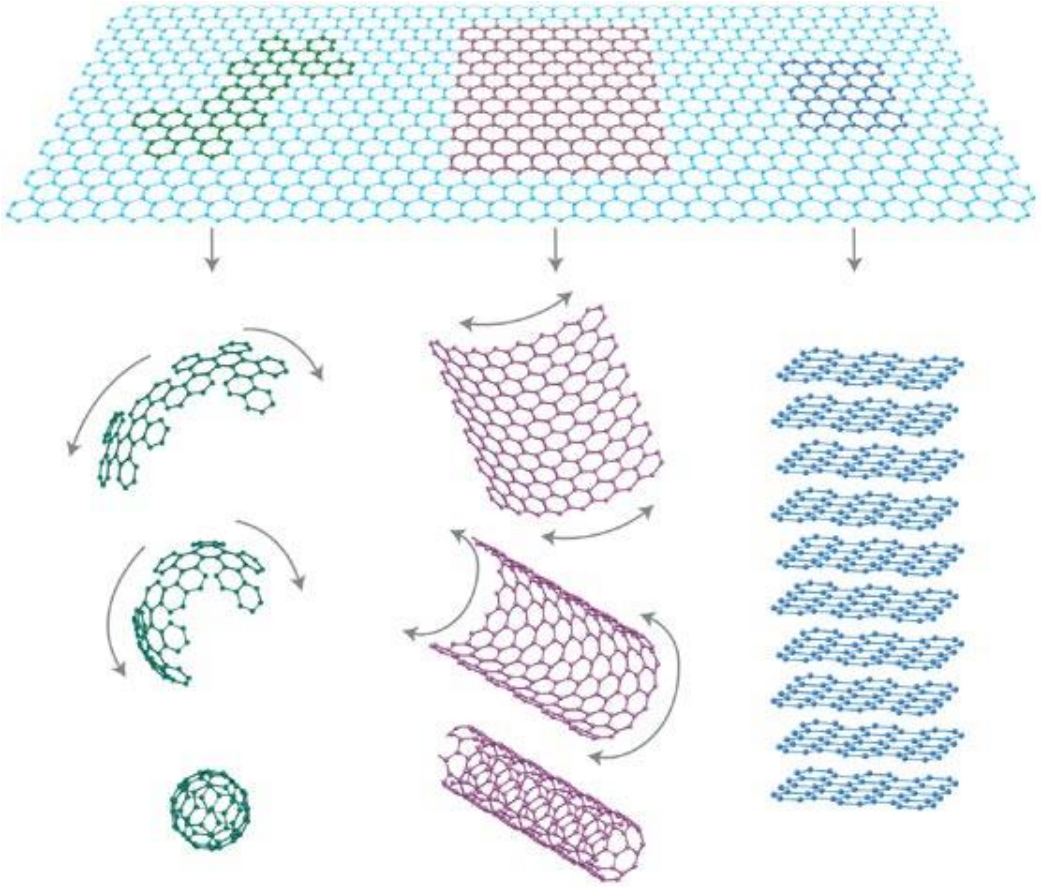

Figure 1. Graphene is a 2-D carbon material. Other allotropes of carbon include 0-D buckyballs, 1-D nanotubes and 2-D graphene and 3-D graphite. (with permission from [1], copyright © 2012 Nature Publishing Group).

1.2 Rise of Graphene

About ten years ago, graphene was shown to be stable as a one-atom thick and two-dimensional carbon allotrope made up of a conjugated system of sp^2 carbons arranged in a honeycomb structure. These studies in 2004 by researchers at the University of Manchester generated graphene by micromechanical exfoliation from a graphite crystal (Andre Geim and Kostya Novoselov won the 2010 Nobel Prize for Physics). [7] These studies ignited considerable interest because of the inexpensive nature of graphite,

the mother material. Before this discovery, graphene was thought to be unstable and that the 2-D lattice would be two reactive to survive outside of its stacked graphite structure.

1.2.1 Structure of Graphene

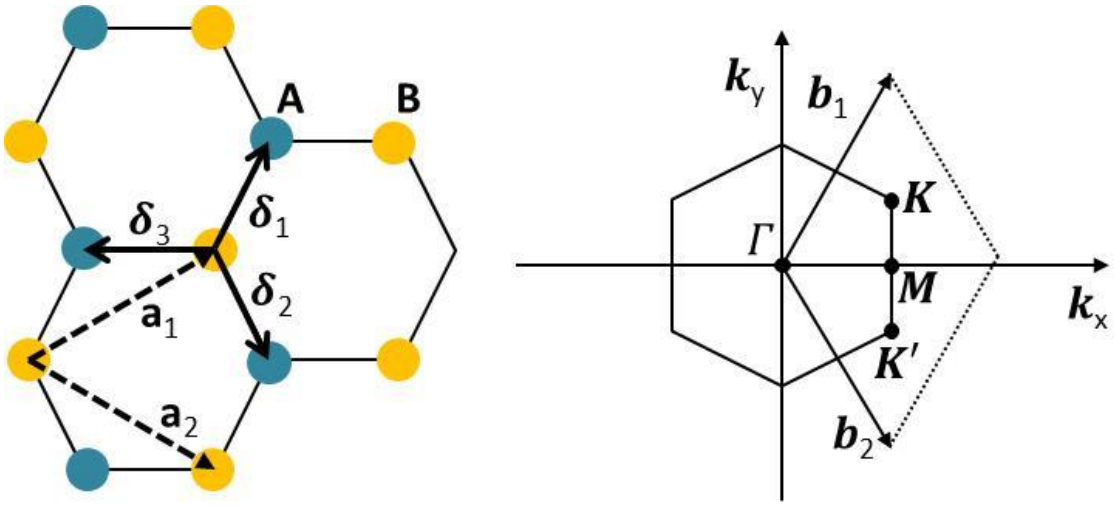

Figure 2. The lattice structure of graphene. The structure of graphene in real space which is made out of two interpenetrating triangular lattice ($\mathbf{a_1}$ and $\mathbf{a_2}$ are the lattice unit vectors, and $\boldsymbol{\delta_i}, \boldsymbol{i} = \mathbf{1}, \mathbf{2}, \mathbf{3}$ are the nearest-neighbor vectors) and its corresponding Brillouin zone. The Dirac cones are located at the **K** and $\mathbf{K}'$ points.

Theoretical studies of the band structure of graphite date back to 1947. [8] The band structure for graphene can be explained by the tight binding approximation. In graphene every carbon atom is bonded with three other carbon atoms via sp^2 hybridized orbitals, which creates strong covalent σ-bonds between neighboring atoms in the hexagonal lattice. The remaining p_z orbitals are delocalized and create π bands of states. The π-type bands have bonding (π-band) and antibonding (π*-band) character. The

structure of a hexagonal lattice of graphene is shown in Figure 2 [9], where $\mathbf{a}_1 = (\sqrt{3}/2,$ 3/2)a, $\mathbf{a}_2 = (-\sqrt{3}/2 ,$ 3/2)a, $\mathbf{b}_1 = 4\pi/3a(-\sqrt{3}/2,$ 1/2)a, $\mathbf{b}_2 = 4\pi/3a(\sqrt{3}/2,$ 1/2)a, and a = 1.42 Å. Each unit cell has two nonequivalent atoms labeled A and B, respectively. In the reciprocal space, the two-atom unit cell results in a Brillouin zone with two conical points at the Fermi surface, K and K' (Dirac points), where the π and π* bands touch in Figure 2. In the vicinity of these points the electron energy is linearly dependent on the wave vector. Consequently, graphene is considered to be a special semi-metal or zero-gap semiconductor. As a result of this unique linear dependence, the electronic properties of graphene are best described by an equation of the form of the relativistic Dirac equation rather than the nonrelativistic Schrödinger equation. This single-layer graphene produces an electronic structure of conical bands with linear dispersion that touch at a point known as the charge-neutrality in Figure 3a. Indeed, in graphene, charge carriers mimic particles with zero mass (Dirac fermions) that effectively have a velocity equivalent speed of light ($v_F \approx 1 \times 10^6$ ms^{-1}), rather than the vacuum value of 3×10^8 ms^{-1}, and mobilities as high as 15,000 $cm^2V^{-1}s^{-1}$ have been reported. [10] In addition, in few-layer graphene, the crystallographic stacking of the individual graphene sheets provides an additional degree of freedom. The distinct lattice symmetries associated with different stacking orders of few-layer graphene have been predicted to strongly influence the electronic properties of few-layer graphene, including the band structure as shown in Figure 3. [11, 12] Bilayer graphene consists of two single graphene layers shifted with respect to each other so that the B atoms of one are situated directly above the A atoms of the other in Figure 3b. This generates an electronic structure that consists of hyperbolic bands, two of which touch at the charge-neutrality point. In trilayer graphene the stacking of the third layer can align

with the first, known as ABA or ABC stacking, whose electronic structure contains both linear and hyperbolic bands in Figure 3c.

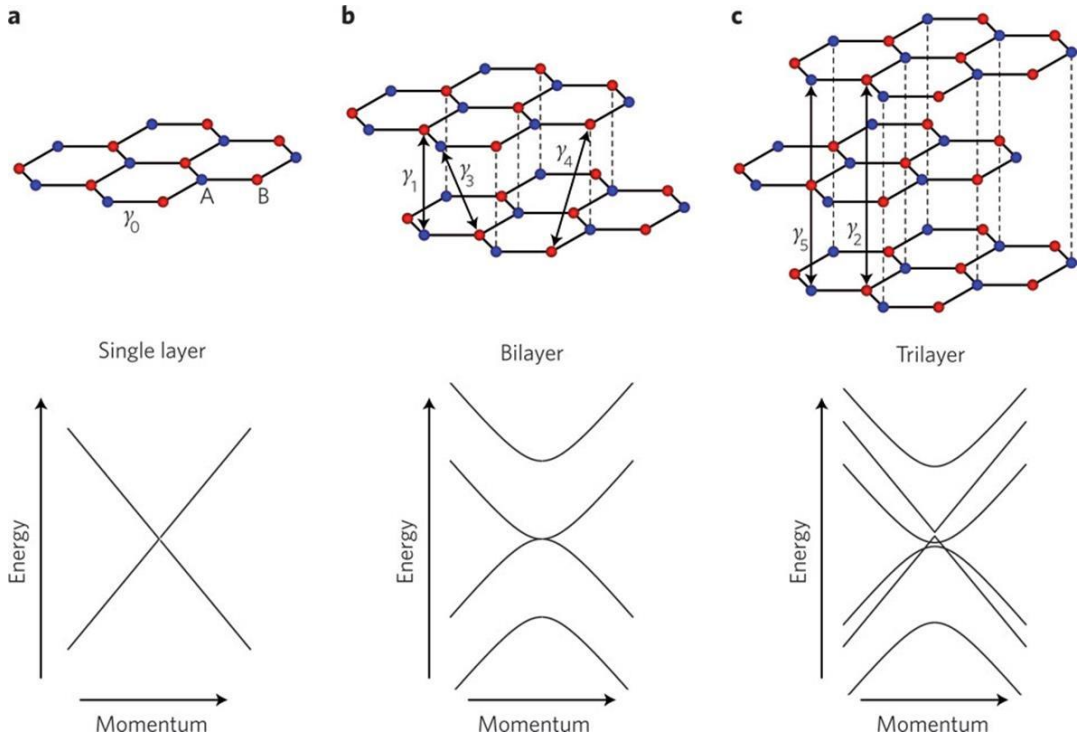

Figure 3. Lattice structure of single, double and trilayer graphene and their band structures. (with permission from [13], copyright © 2011 Nature Publishing Group).

1.2.2 Chemistry of Graphene

Surface chemistry is critical to both the chemical and physical properties of graphene as well as the real-world applications of this material. [14, 15]. However, to realize this great potential for various applications, there are still some major shortcomings that limit its successful application to commercial applications. A basic and very important property is the solubility/dispersability of the graphene. The physical manipulation/processing of graphene sheets is challenging since graphene agglomerates

are insoluble in water and organic solvents. Studies on the solubility of graphene in aromatic solvents relative to other solvents have been conducted in terms of the solvent Hansen/Hildebrand solvent solubility parameters and surface tension. [16] Although these studies provide some understanding of the interaction between graphene and organic solvent, the actual mechanism of graphene dispersion in these solvents is still not known. For example, N-Methyl-2-pyrrolidone (NMP) is the eighth best solvent based on the solubility parameter. However, it is the best solvent in terms of exfoliation and stability. Second, the Dirac fermion nature of graphene has provided superior electrical conductivity, but this also limits graphene's utility in field effect transistors (FET) because a completely off state is not readily achieved leading to a small on/off current ratio. Hence, a zero energy gap graphene is unsuitable for transistor applications.

Chemical functionalization of graphene is an approach to address the challenges for the development of graphene technologies. The detailed reactivity of graphene sheets, in terms of size, shape, and stoichiometric control, is not well understood. In general, graphite is known as a chemically inert material and perfect graphene sheets are in theory very stable structures that are not susceptible to chemical functionalization. Several chemical procedures have been developed to produce dispersible graphene by adding functional groups to a graphene. [17] Additionally, defects are always present in graphene and these sites can be utilized for functionalization. Chemical doping also offers possibilities and can introduce a band gap near graphene's Fermi level to create a semiconductor. Chemical functionalization can also allow for the preparation of p- and n-doped graphene based on the selection of electron donating or withdrawing complexes covalently bonded to the graphene carbons. For example, if graphene is covalently

bonded to electron-withdrawing oxygen containing functionalities, p-doping can be induced. Similarly, if it is functionalized by electron-donating nitrogen functionalities, n-doping can be achieved. [6] Additionally, the hydrogenation of graphene, which involves the change of the carbon atom's electronic structure from sp^2 to sp^3, results in a conversion of graphene into an insulating material. [18] Fluorine addition can similarly modify the electronic properties of graphene by reducing the charge in the conducting π orbitals, by introducing scattering centers, and by opening band gaps. [19]

The common covalent functionalization methods used for the chemical modification of graphene can be divided into two general categories: (1) the formation of covalent bonds directly on the carbon atoms through nucleophilic addition, cycloaddition, free radical addition (aryl diazonium salt), substitution (reaction with electrophiles), and (2) reactions of graphene oxide such as Claisen rearrangements and/or the formation of covalent bonds to pendant organic or oxygen groups. [17, 20] This knowledge of graphene chemistry provides valuable insight into its reactivity, and ultimately, its properties. Improvements in synthetic modifications of graphene are certain to enable promising opportunities with graphene.

1.3 Applications of Graphene

Graphene is undoubtedly a fascinating building block from which to develop two-dimensional (2-D) nanotechnology. Its intriguing combination of unusual properties, as well as the enormous potential commercial applications, has attracted the widespread interest of the scientific and engineering communities. Advances in graphene science and technology depend critically on finding and manipulating new forms of graphene into

functional materials. The interest in graphene can be attributed to the following reasons: The great versatility of graphene materials arises from the strength of their sp^2 bonds. First, their π-electron transport is described by the Dirac equation, which has proved to be an excellent test of quantum field theory as applied to condensed matter experiments. [10, 21] Second, the scalability of graphene devices to nano-dimensions ballistic transport at room temperature combined with chemical and mechanical stability makes it a promising candidate for applications. Graphene's remarkable properties extend to bilayer and few-layers graphene. The most common techniques available for the synthetic technologies of graphene are shown schematically in Figure 4. These methods include micromechanical cleavage, chemical vapor deposition (CVD), epitaxial growth, chemical reduction of exfoliated graphene oxide, and liquid phase exfoliation of graphite. [22, 23] Each synthetic possesses has intriguing features that make it attractive for a broad range of applications that leverage its electronic, mechanical, thermal, and/or transport properties. These attractive features of graphene depend on the synthetic methods used to functionalize the system and expanding applications include sensors, energy conversion and storage devices, electronics and transparent electrodes for displays, and solar cells. To improve the quality and availability of synthetic graphene requires new synthetic methods for large scale production and high quality graphene via simple and cost effective approaches.

1.3.1 Flexible, Stretchable and Foldable Nanoelectronics

The advances in graphene engineering provide several promising engineering options for stretchable and foldable nanoelectronics. [24, 25] Some of the most promising

applications of graphene are for the creation of electronic components such as transistors and interconnects. Truly foldable and flexible electronics require a foldable and bendable substrate and a stable and durable conductor that can withstand folding that can develop creases, and deformations that can recover after unfolding. Graphene, which has characteristic mechanical flexibility, high electrical conductivity, and chemical stability, has the potential to produce new generations of electronics that move from hard, rigid, and planar chips, to soft, stretchable, and foldable sheets. Indeed, highly flexible and stretchable conducting transparent devices have already been developed with graphene. [26-28]

Method	key features	Applications
Mechanical exfoliation (5 to 100 μm)	• Small scale production • High cost • High Quality • Uneven films	• Research Purpose
CVD (nm to few μm)	• Moderate scalability • High cost • High quality • High process temperature (>1000°C)	• Touch screens • Smart windows • Flexible LCDs, & OLED • Solar cell
Epitaxial Growth (>50 μm)	• Low yield, High cost • High Quality • High processing temperature (>1500°C) • Very expansive substrate	• Transistor • Circuits • Interconnects • Memory
Liquid-based method (nm to a few μm)	• High scalability • Low yield • Moderate quality • low cost, impure	• Polymer fillers • Transparent electrodes • Sensor • Energy application
Chemical Reduction of graphene oxide (nm to a few μm)	• High scalability • Low cost • Low purity • High defect density	• Conductive inks • Polymer fillers • Battery electrodes • Supercapacitor, sensor

Figure 4. A graphic showing the most common available techniques used for the synthesis of graphene along with their key features, and applications.

1.3.2 Sensors

Graphene has shown excellent utility for direct electrochemistry with enzymes, electrochemical detection of small biomolecules, [29, 30] pH sensors, [31] gas sensors [32] and flexible strain sensors. [33] Graphene has potential use in gas sensors as a result of the extremely high surface area of its 2-D structure. [34, 35] Graphene's electrical conductivity can be altered when molecules interact with its π-electron surface to either pin or scatter carriers of donate/withdraw electron density to/from the π-bands. Graphene can reversibly endure strains of over 30% and graphene-based strain sensors have been developed. [36] This property can be useful to create wearable human-interfaced electronics. In summary, improved understanding of graphene's physics and chemistry and its interaction of chemicals and bio-molecules will enable a wide range of sensor applications.

1.3.3 Energy

Three-dimensional networks of highly curved, one atom thick walls of graphene are theoretically predicted to have specific surface areas of up to 2630 m^2/g with very high intrinsic electrical conductivities, high mechanical strength, and chemical stability. [37] Therefore, graphene-based nanomaterials have many promising applications especially in energy conversion and storage (solar cells, Lithium ion batteries and supercapacitors). Graphene solar cell electrodes promise to be inexpensive, lightweight, flexible and multifunctional. [38, 39] In addition, it recently has been proposed that graphene is a competitive material for supercapacitor applications with both high gravimetric and volumetric specific capacitance (> 100 F/g). [40-42]

1.4 Challenges in Production

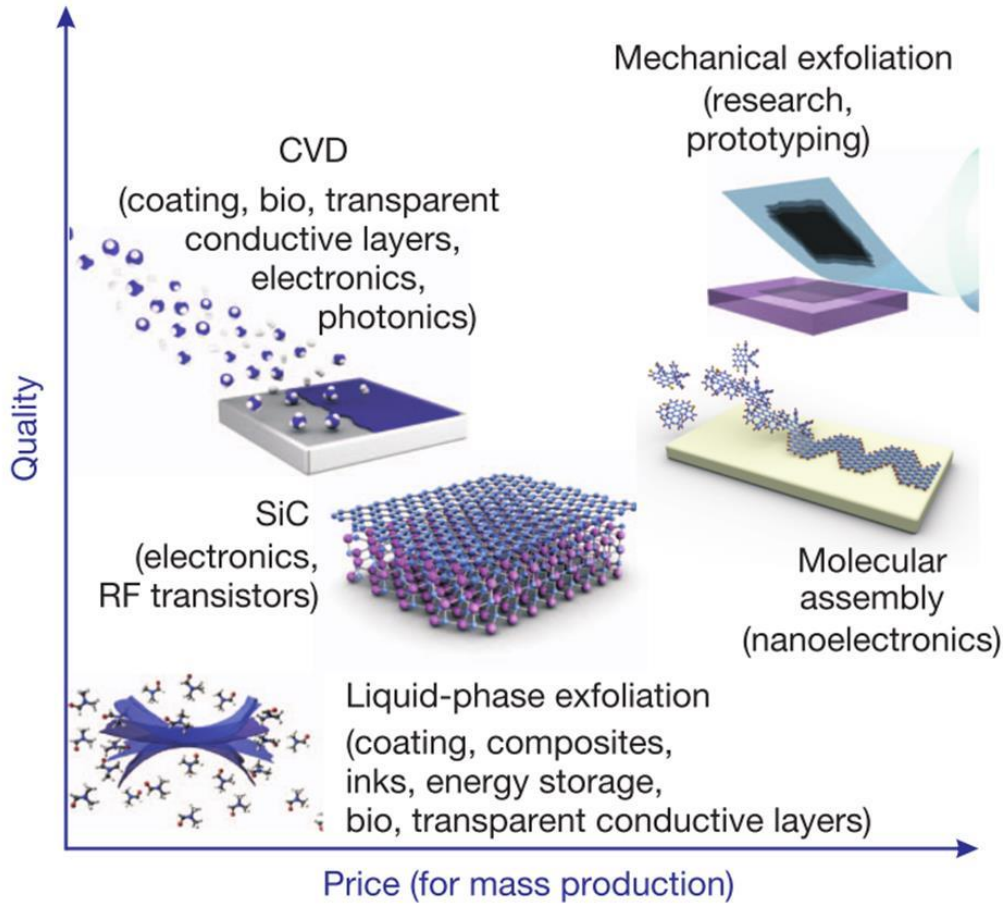

Figure 5. The properties of a particular grade of graphene (and the pool of applications) depend on the quality of the material, type of defects, substrate, and so forth, which are strongly affected by the production method. (with permission from [23], copyright © 2012 Nature Publishing Group).

Single-layer graphene is currently produced either by a laborious micromechanical exfoliation or CVD or through high-temperature reduction of silicon carbide. These methods produce very small quantities of graphene and mass production and defect engineering have been major issues. In short, producing high-quality defect-free graphene is time-consuming and expensive. Figure 5 shows the categorization of

graphene by the quality of the graphene and the potential applications. The properties of a particular grade of graphene are strongly affected by the method of production. We review briefly recent technologies in the development of production methods.

1.4.1 Micromechanical Exfoliation of Graphene

In the micromechanical exfoliation method, highly oriented pyrolytic graphite (HOPG) is repeatedly pealed from a surface using adhesive tape and deposited onto a silicon substrate. Micromechanical exfoliation yields small samples of randomly distributed individual graphene sheets. This fabrication scheme is only useful for research purposes. Drawing with a pencil creates lines containing many graphene sheets spread over paper. This approach is attractive from a patterning standpoint but unfortunately is uncontrollable generating many sheets of varying thicknesses.

1.4.2 High Temperature Deposition

CVD (chemical vapor deposition) is a method for graphene manufacturing on catalytic metal films. Large-area uniform polycrystalline graphene films have been produced by this process on copper foils and germanium wafers with minimal defects. [43, 44] At present, the process is expensive owing to its large energy consumption. Furthermore, this method requires intensive post-processing (e.g. transfer process) to transfer the graphene from the metal to the surface of substance. This process is also complicated as the quality of graphene can degrade as a result of wrinkles or cracks. The transfer process requires improvements that minimize damage to the graphene and of recovery of the metal. [23] Heating the SiC crystals to high temperature sublimes Si

atoms and produces a few layers of graphene/graphite on the substrate. [45] The quality of such graphene can be very high, with crystallites approaching hundreds of micrometres in size. However, the drawback is the high cost of the SiC wafers and the high temperatures (> 1,000^{o}C) used, which are not directly compatible with conventional silicon electronics. Therefore, neither of the two approaches has yet been scaled to large scale applications.

1.4.3 Liquid-based Process

In the past decade enormous efforts have been devoted to the low-cost liquid phase exfoliation of graphite to produce pristine graphene. The most common bulk production of graphene is to disperse graphene into solvents. Exfoliation methods that do not involve strong oxidants or high temperatures have the prospects for creating high quality materials. A common approach is to sonicate graphite powders in an organic solution and then to deposit the dispersion on a surface. [46] However, this method has limitations in that the obtained graphene 1) exhibits high polydispersibility in terms of the number of layers and lateral dimensions, 2) requires expensive exfoliating media with high boiling points, 3) the surfactants often deployed are difficult to remove and 4) long sonication times are required which can reduce the size of the resultant graphene sheets and introduce defects. In addition, the techniques are limited as a result of the chemistry required to keep individual graphene sheets from aggregating in solution. However, solution processing of pristine graphene based films has great potential for the cost-effective production of surface coating, composites, flexible electrodes, sensors, mechanical resonators, and separation membranes.

1.4.4 Reduction of Graphene Oxide

In most studies graphite oxide is synthesized through an acid/oxidation treatment of graphite by the Hummers method. [47] Graphene oxide may also expose to either thermal or mechanical treatments to create different types of materials. [48] The oxidative reactions result in the formation of various oxygenated groups including carboxylic acids, ketones, and hydroxyls. Although graphene oxide offers routes to diverse and dispersible graphenes, the degradation of the carbon lattice under the Hummer's reaction conditions is extensive. Graphene oxide is invariably highly defective and its electrical conductivity is several orders below that of graphene even after thermal and chemical reduction. The graphene domains have irregular edges and even random holes through the carbon sheets. [46, 49] The numerous defects in graphene oxide produces largely electrically insulating materials and an additional chemical reduction step is required to best restore an extended π-network. [15]

Chapter 2.

Electrochemical Expansion of Graphite

2.1 Introduction

As detailed in Chapter 1, graphene suffers from a lack of effective methods for large-scale production and processing into high performance materials. Consequently, there is a need for methods that produce large quantities of graphene with low defect densities that can be processed. The nondestructive electrochemical exfoliation of graphite via the formation of intercalation compounds is extremely attractive because these processes generate low-defect level graphenes that are potentially scalable. In addition, electrochemical expansion constitutes a feasible option for the liquid phase production of few-layer graphenes with minimal energy requirements. The primary aim of this thesis is to develop electrochemical treatments of graphite for the fabrication of graphene and other graphitic nanomaterials. The approach is to develop and optimize intercalative expansion of graphite, as well as subsequent diazonium functionalizations.

2.2 Intercalation of Graphite

Electrochemical methods have been used for the synthesis of graphite intercalation compounds. [50] Graphite intercalation compounds are defined as compositions wherein atomic or molecular layers of a different chemical species, called the intercalant, are inserted between layers of the graphite host material. Intercalation in graphite implies that the guest species between carbon layers leaves the graphene layers intact (i.e. a pure undistorted sp^2 lattice), and intercalation leads to different interlayer distances. Our exfoliation methods make use of graphite's intercalative properties and were also inspired by electrochemical reactions of negative graphite electrodes in liquid-rechargeable lithium ion batteries.

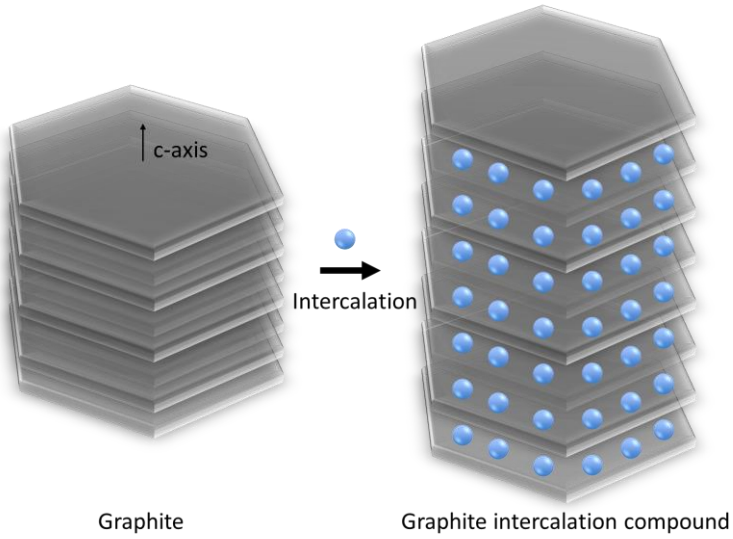

Figure 6. Structure of graphite and graphite intercalation compound. Left: schematic drawing showing the layered stacking graphite. Right: simplified representation of intercalated graphite. Blue sphere indicates intercalant (e.g. Li^+ ion or other intercalant molecules).

Lithium intercalated graphite has been studied previously to give exfoliated graphene layers by electrochemical STM [51, 52]. Specifically, these studies revealed that charging graphite in $LiClO_4$/PC electrolyte resulted in rapid exfoliation and rupturing of graphite layers to affect intercalation as shown in Figure 6. Intercalation causes crystal expansion along the c-axis. Larger molecular intercalants generate larger dilatation for compounds of comparable stage. In general, both the chemical affinities and geometric constraints associated with intercalant size and intercalant bonding distances determine whether or not a given chemical species will intercalate. These factors are critical to understand in order to disaggregate graphite into individual graphene monolayers.

2.2.1 Structure of Graphite Intercalation Compounds

Graphite substrates, such as highly oriented pyrolytic graphite (HOPG), offer an appropriate structure for ionic, atomic and molecular species to diffuse between the layers and to form intercalation compounds. [53] During electrochemical charging in a graphite electrode Li^+ ions are reversibly intercalated into the graphite interlayers. In these systems the maximum lithium content is one Li guest atom per six carbon atoms for highly crystalline graphite. With lithium intercalation the interlayer distance between the graphene layers increases moderately (10.3%, c=0.37 nm). [54] In LiC_6 the lithium is distributed in-plane and Li atoms occupy the space above and below the center of only every third hexagonal ring in the graphitic layers resulting in an overall chemical composition of LiC_6. [55] However, a common opinion is that the formation of LiC_n in graphite matrix is not solely responsible for graphite expansion and that propylene carbonate solvent molecules cointercalate with Li^+. [56] A loss of reversibility arises with

solvent cointercalation and exfoliation of the graphite. [57] It has been proposed that cointercalation of PC with Li^+ to form a ternary graphite intercalation compound, $Li_x(solv)_yC_n$, exerts considerable interlayer stress at the edge of the graphite interlayers that results in cracking and exfoliation of the graphene planes. [57, 58] The failure of graphite electrodes in the pure PC electrolytes have been attributed to a lack of an effective solid electrolyte interface (SEI) compounds on the graphite surface, and the decomposition of solvated graphite intercalation compounds to produce propylene gas inside the graphite. Although these processes are problematic in Li ion batteries, they have relevance and potential advantage for the electrochemical exfoliation of the graphite.

2.2.2 Interlayer Binding in Graphite

It is a challenge to theoretically describe the van der Waals interactions in graphitic materials, and extensive work is still needed for better understanding of the interlayer cohesion and intercalation process in graphite in both theoretical and experimental terms. [59] The molecular attractive forces between adjacent layers of graphite are relatively weak and can be surmounted by external forces. These forces can also be weakened by increasing the interlayer distance between the graphite layers, since the van der Waals force is roughly proportional to $-1/r^6$, where r is the distance between the molecules. Density functional theory calculations (local density approximation (DFT-LDA) predict that the van der Waals force of AB stacking graphite approaches zero for interlayer spacing greater than 5 Å. [60] Hence, if we can achieve this interlayer distance and the reduction of interlayer binding energy of graphene layers through intercalation, only mild sonication should be required to produce graphene flakes.

2.2.3 Recent Research

A summary of previous electrochemical exfoliation research is listed in Table 1. These previous studies demonstrate that electrochemical exfoliation of graphite furnishes graphene sheets in high quality and high yield.

Table 1. Comparison of electrochemical approaches to produce graphene sheets.

Starting materials	Set up	condition	Duration	Electrolyte	Sonication condition	Raman spectra	Result	Ref.
Graphite gasket	Two electrode (Pt)	-3.0 V to -5.0	24 hr	$LiClO_4$ /TBA^+/PC	DMAc	After BrBD treatment[a] I_D/I_G=1.1	.	[62]
Graphite powder	Two electrode (Pt)	-15 ± 5 V	.	$LiClO_4$/PC	LiCl/DMF/ TMA/PC for >10 hours	I_D/I_G<0.1	<5 layers	[61]
HOPG	Three electrode	-5.0 V	3 hr	TBA/NMP	NMP for 6 h	.	few layer	[63]
Graphite flakes	Two electrode (Pt)	<10 V At 25°C	.	H_2SO_4/KOH pH~1.2 to pH~7.2	DMF for 5 min	I_D/I_G>1	>60% bilayer	[64]
Graphite flakes	Two electrode (Pt)	+10 V	2 min	H_2SO_4	DMF for 10 min	I_D/I_G=0.4	> 80% < 3 layer	[65]

[a]Treatment with 4-bromobenzenediazonium (BrBD) results in functionalization of exfoliated and activated graphene.

A figure of merit for the degree of exfoliation and activation of the graphene shown in Table 1 is the degree of covalent functionalization by reaction with diazonium reagents. These reactions create non-sp^2 carbons and give an increase in the D-band (disorder-band) in the Raman spectra relative to the G-band (graphite-band). Despite these successes, there are issues to be resolved. Wang et al. showed exfoliation of graphite into few-layer graphene flakes via the intercalation of Li^+ complexes, further enhanced the graphite expansion by adding additional ions, and then subsequently

sonicated the intercalated compounds. [61-63] However, these studies employed extreme potentials (-15±5 V), excessively long sonication times for exfoliation and extensive rinsing to remove Li atoms. H_2SO_4 solution based electrochemical exfoliation methods produce materials with large sheet resistances and oxygen content. [64, 65] Clearly, these methods are not compatible with mass-produced graphene that matches the performance of the best samples obtained by CVD.

2.3 Experiments

2.3.1 Chemicals and Materials.

An economical source of graphite is commercial gaskets that are 1/32" and 1/8" thick from John Crane's Crane-foil^{TM}. The following chemicals were obtained from Sigma-Aldrich and used without further purification: propylene carbonate (PC, anhydrous, 99.7%), tetrabutylammonium perchlorate (TBAP, for electrochemical analysis, ≥99.0%), and 4-nitrobenzenediazonium tetrafluoroborate (97%), N-methyl-2-pyrrolidinone (NMP, 99.5 %), and acetonitrile (anhydrous, 99.8 %), ethyl acetate (99.5 %), Millipore distilled water (18.2 MΩ·cm) was used for sample rinsing and preparation of all aqueous solutions.

2.3.2 Experimental Methods and Characterization

An electrochemical cell was created with a graphite gasket as the negative working terminal, a platinum mesh as the positive counter electrode, and a Ag/Ag^+ reference electrode. Electrochemical analysis for the expansion and exfoliation were

performed using an Autolab PGSTAT 30. The expanded graphite was ultrasonicated using ¼ in. Branson micro-tips. X-ray powder diffraction (XRD) was recorded with PANalytical X'Pert Pro Multipurpose diffractometer with the Cu Kα radiation (45 kV, 40 mA) line. Scanning electron microscopy (SEM) images were obtained on a JEOL 6010A. Transmission electron microscopy (TEM) images were obtained with a JEOL 2010F microscope at an acceleration voltage of 200 kV. The samples were supported on a Lacey carbon only Cu TEM grid. X-ray photoelectron spectroscopy (XPS) was performed with the Physical Electronics Versaprobe II X-ray Photoelectron Spectrometer equipped using an unmonochromated Al Kα X-ray source (1486.6 eV). The UV-vis absorption and photoluminescence measurements were performed on a Varian Cary 6000i spectrophotometer. Raman Spectroscopy was performed with a Horiba Jobin Yvon HR800 micro-Raman system with a 532 nm excitation laser (laser spot size of 1 μm) operated at a low power level in order to avoid any heating effect. Prior to use, the Raman spectrometer was calibrated using the standard 521 cm^{-1} band of Si. The graphene in NMP was coated onto a Si/SiO_2 substrate for Raman measurements. The sheet resistance was measured by a four-point probe (Keithley Model 2400). Thermogravimetric analysis was done at TA instrument TGA Discovery at 50-900^{0}C under nitrogen with the heating rate of 10^{o}C/min.

2.3.3 Electrochemical Set-up and Electrochemical Procedures

In present work we demonstrate a one-step process wherein graphite is first activated in tetrabutylammonium (TBA) containing propylene carbonate (PC). Based on calculations, the intercalate diameter of tetrabutylamommonium ion is 0.826 nm, the

diameter of tetrametylamommonium ion is 0.558 nm, and the diameter of tetraetylamommonium ion is 0.674 nm. All of these are larger than the interlayer spacing of graphite (0.354 nm). [66, 67] Propylene carbonate (PC) has been used as our solvent and it has been a very popular solvent for Li ion batteries. High intercalation/deintercalation efficiency has been reported when lithium perchlorate/propylene carbonate ($LiClO_4$/PC) is used as the solvent-supporting electrolyte system. [68] It is now well known that PC decomposition can occur on graphite material during the charging process. Because of this, destructive behavior can lead to rapid exfoliation and rupturing of the graphite layers. [51] However, the yield of dispersed graphene in PC remains low and the majority of the exfoliated graphene flocculates in a few hours in the PC solvent. It remains a challenge to generate defect free well-disperse graphene sheets because graphene is not soluble/dispersable in most solvents. Graphene is only soluble/dispersable in solvents exhibiting surface tension close to 40–50 mJ/m. Although the exact mechanism of graphene dispersion in these solvents is still not known, Hernande et al. suggested a good criterion and have identified promising solvents based on Hansen solubility parameters. [16] The Hansen solubility parameters are the square roots of the dispersive, polar, and hydrogen bonding components of the cohesive energy density of a material and are denoted as δ_D, δ_P, and δ_H, respectively. Hansen has suggested that the enthalpy of mixing is given by $\Delta H_{mix}/V_{mix} \approx \left[\left(\delta_{D,S} - \delta_{D,G}\right)^2 + \left(\delta_{P,S} - \delta_{P,G}\right)^2/4 + \left(\delta_{H,S} - \delta_{H,G}\right)^2/4\right]\phi_G$, where the subscripts S and G represent solvent and graphene, respectively. Where $\Delta H_{mix}/V_{mix}$ is the enthalpy of mixing of graphene per volume of solvent. The Hansen parameters for graphene are $\delta_{D,G} \approx 18.0$ $MPa^{1/2}$, $\delta_{P,G} \approx 9.3$ $MPa^{1/2}$, and $\delta_{H,G} \approx 7.7$ $MPa^{1/2}$ in Table 2.[16] N-methyl-pyrrolidone (NMP), which

has a specific surface tension (40.79 mN/m) as well as the appropriate Hansen solubility parameters, is suitable for graphene dispersion.[16] As a result, NMP was chosen for graphene dispersion after electrochemical exfoliation.

Table 2. Hansen parameters for graphene and various solvents [69]

Materials	δ_D	δ_P	δ_H
Graphene	18	10	7
Propylene carbonate	13.3	9.8	8.8
N-methyl-pyrrolidone	18	12.3	7.2
Benzyl benzoate	20.0	5.1	5.2
Cyclopentanone	17.9	11.9	5.2
Cyclohexanone	17.8	8.4	5.1
N-formyl piperidine	18.7	10.6	7.8
Vinyl pyrrolidone	16.4	9.3	5.9
1,3-Dimethyl-2-imidazolidinone	18	10.5	9.7
Bromobenzene	19.2	5.5	4.1
Benzonitrile	18.8	12	3.3
NN′-Dimethylpropylene urea	17.8	9.5	9.3
γ-Butrylactone	18	16.6	7.4
Dimethylformamide	17.4	13.7	11.3
N-ethyl-pyrrolidone	18	12	7
Dimethylacetamide	16.8	11.5	9.4
Cyclohexylpyrrolidone	18.2	6.8	6.5
DMSO	18.4	16.4	10.2
Dibenzyl ether	19.6	3.4	5.2
Chloroform	17.8	3.1	5.7
Isopropylalcohol	15.8	6.1	16.4
Cholobenzene	19	4.3	2
1-Octyl-2-pyrrolidone	17.4	6.2	4.8
1-3 dioxolane	18.1	6.6	9.3
Ethyl acetate	15.8	5.3	7.2
Quinoline	20.5	5.6	5.7
Benzaldehyde	19.4	7.4	5.3
Ethanolamine	17.5	6.8	18
Diethyl phthalate	17.6	9.6	4.5
N-Dodecyl-2-pyrrolidone	17.5	4.1	3.2
Pyridine	19	8.8	5.9
Dimethyl phthalate	18.6	10.8	4.9
Formamide	17.2	26.2	19
Ethanol	15.8	8.8	19.4
Vinyl	16	7.2	5.9
Acetone	15.5	10.4	7
Water	15.5	16	42.3
Ethylene glycol	17	11	26
Toluene	18	1.4	2
Heptane	15.3	0	0
Hexane	14.9	0	0

Pentane	14.5	0	0
Ethylene carbonate	19.4	21.7	5.1

Our activation of graphite gasket begins with the immersion of a strip of graphite in propylene carbonate solvent containing tetrabutylammonium (TBA) ions. The graphite is then connected to the negative terminal of a potentiostat via a flat alligator clip and a platinum mesh was employed at the positive terminal in Figure 7. A silver/silver nitrate non-aqueous reference electrode ($Ag/AgNO_3$) was used for reference electrode.

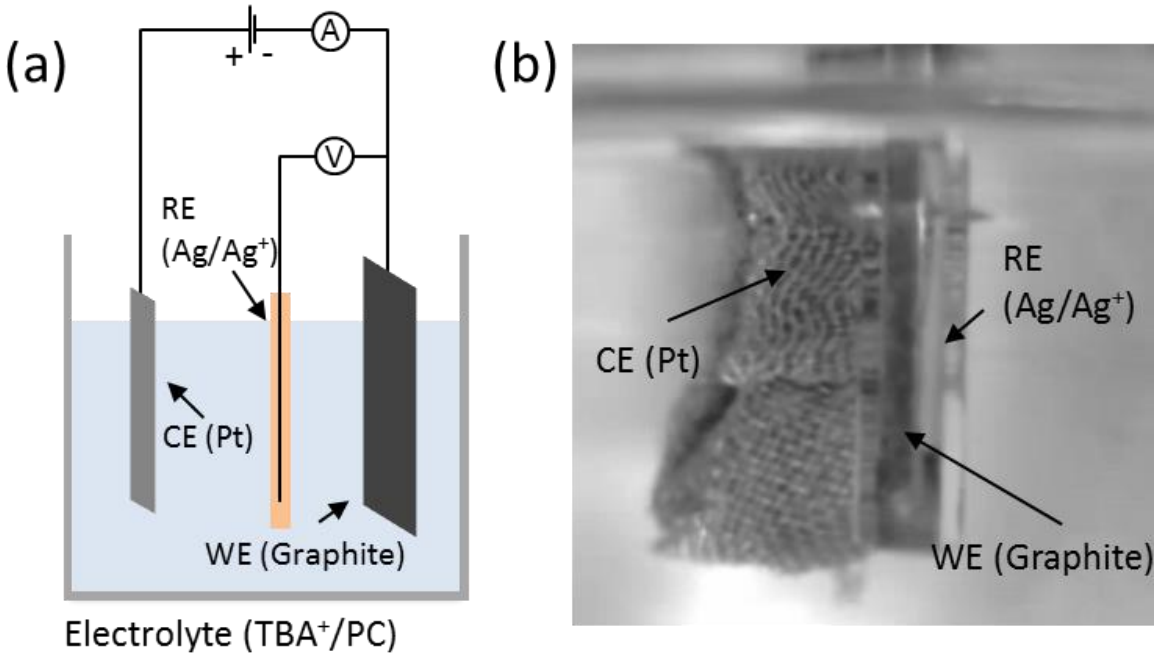

Figure 7. (a) Schematically illustrates experimental exfoliation setup, where graphite gasket or graphite foil was employed as a working electrode (WE) and source of graphene for electrochemical exfoliation. A Pt mesh was chosen as a counter electrode (CE) and Ag/Ag^+ reference electrode (RE) is used. (b) A photo of an actual electrochemical cell viewed from the WE (foreground) toward the CE.

The major challenge in achieving the full expansion of graphite is to overcome the van der Waals energy contained in π–π stacked graphene sheets of a graphite crystal. According to binding energy of AB-stacked graphite as a function of interlayer distance, an interlayer separation of >0.8 nm is required to minimize π-interaction energy of graphene to allow efficient exfoliation [70] Therefore, intercalation of TBA^+ ion into the graphite lattice (the crystallographic ionic diameter: ~0.8 nm) is expected to effectively separate graphene layers, although the ionic diameter is expected to be reduced to 0.47 nm as a result of a conformational distortion of the TBA^+ ions between layers. [71] As a result, electrolyte solutions containing tetrabutylammonium were used and potential is decreased linearly (-2.8 mV/min) form -1.8 V to -2.22 V, and an associated physical expansion of the graphite is observed. In this step, the graphite gasket expands along its c-axis as a result of the co-intercalation of PC with TBA^+ ions.

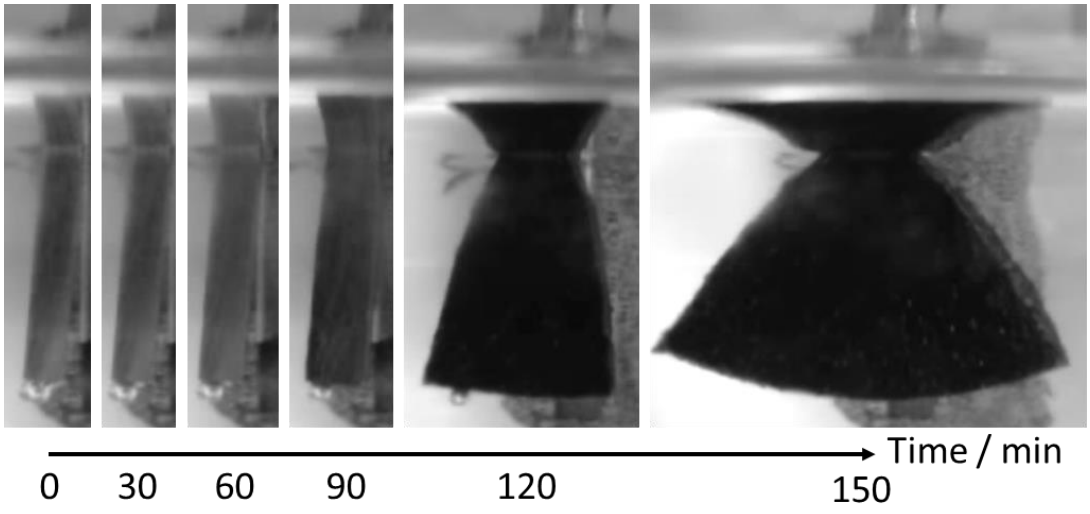

Figure 8. Snapshots of expanding of graphite gasket. The time interval between two adjacent frames is 30 mins. A physical increase in the volume of the expanded graphite is observed due to the intercalation of TBA^+ ions and solvent.

Figure 8 shows a typical expansion of graphite gasket in electrolyte when a negative potential is applied. Similar to the Li^+/PC electrochemical exfoliation system, co-intercalation of TBA^+ ions and PC results in the electrochemical exfoliation of the graphite. As a result of the flexibility of the alkyl groups and the TBA^+ ions, these ions diffuse into graphite matrix under mild conditions. [71] A slow increase in potential is required to keep the carbon electrode intact and finish the exfoliation at a final potential of -2.22 V vs. $Ag/AgNO_3$. If the ramping rate of potential is fast rupturing occurs and small graphite flakes are generated as a result of stresses caused by uneven distributions of intercalated ions inside the graphite. A visible expansion along the c-axis was observed above 2.0 V vs. $Ag/AgNO_3$.

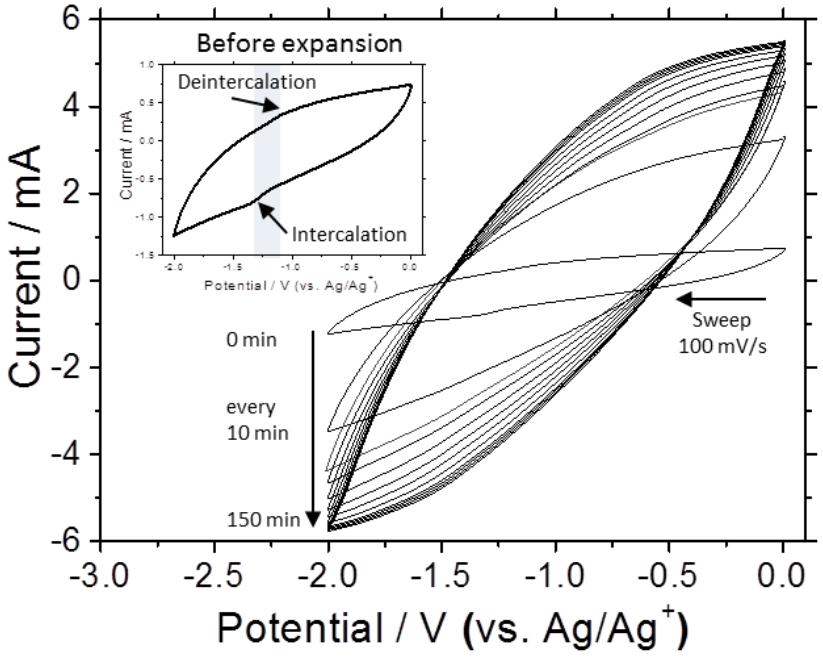

Figure 9. Cyclic voltammograms recorded between 0 and -2 V at a scan rate of 100 mV/s after the graphite as the negative electrode had been precharged at potentials from -1.8 to -2.2 V. The inset is a cyclic voltammograms before expansion.

Figure 9 shows cyclic voltammogram displaying a capacitive current from the expanded graphite electrode that increased with the charging voltage throughout the electrochemical expansion. Co-intercalation of propylene carbonate with TBA^+ ions forms solid-electrolyte-interphase (SEI) layers that stabilize the expansion of graphene after a reduction in electrochemical potential. During the first cyclic voltammetry scan from 0 to -2 V a broad cathodic peak current at -1.4 V is observed that is associated with the intercalation of TBA^+ into the interlayer of graphite (Figure 9). Subsequently, on the reverse scan (-2 to 0 V) a small anodic peak current at -1.2 V also is observed that is expected with the de-intercalation of TBA^+. The structurally reversible process observed is thought to involve intercalation/deintercalation. However, no significant visible expansion/contraction was observed through an optical camera. A typical voltage ramp was as follows: -1.8 V to -2.22 V at a voltage step of -0.028 V every 10 min. Cyclic voltammograms recorded between 0 and -2.0 V at a scan rate of 0.1 V/s after the graphite electrode had been precharged at potentials from -1.8 to -2.22 V. We found that the capacitive current of the expanded graphite increased with the charging voltage and associated electrochemical induced expansion. Under these mild conditions gas evolution of propylene was not detected in contrast to the previously reported high-voltage electrochemical charging methods. [61]

Chapter 3.

Characterization of Expanded Graphite

3.1 Structure Characterization

The physical form and morphology of our electrochemically exfoliated graphene was recorded optically throughout the process and after expansion by SEM as shown in Figure. 10. Figure 10b to 10d detail the microstructure of the graphene as having a loose and porous structure resulting from the expansion of the graphene networks at the surface edges wherein the electrochemical intercalation begins. Higher magnification images (bottom of Figure 10), reveal that the graphite gasket transforms to a loose porous structure with an increase in interlayer spacing. However, the graphene sheets are likely still experiencing weak interlayer van der Waals forces until the intercalation forces a sufficient interlayer spacing. As a result, dry sample preparations of intercalated graphite the graphene sheets can re-aggregate. In Figure 10d-1 the bright contrast at the edge of graphite indicates that the sheets are disassembled from neighboring graphene layers. The intercalation reduced interfacial energy between graphene sheets enables effective dispersion by sonication. Concentrated graphene solutions of 0.1 mg/mL were prepared by dispersing the expanded graphite in NMP by tip sonication for 30 min. The resultant

graphene solutions were then centrifuged at 2000 rpm for 30 min. After centrifugation the top 80% of the supernate dispersion was collected. No significant sedimentation was observed after two weeks of standing and the solution still displays a Tyndall effect (Figure 10).

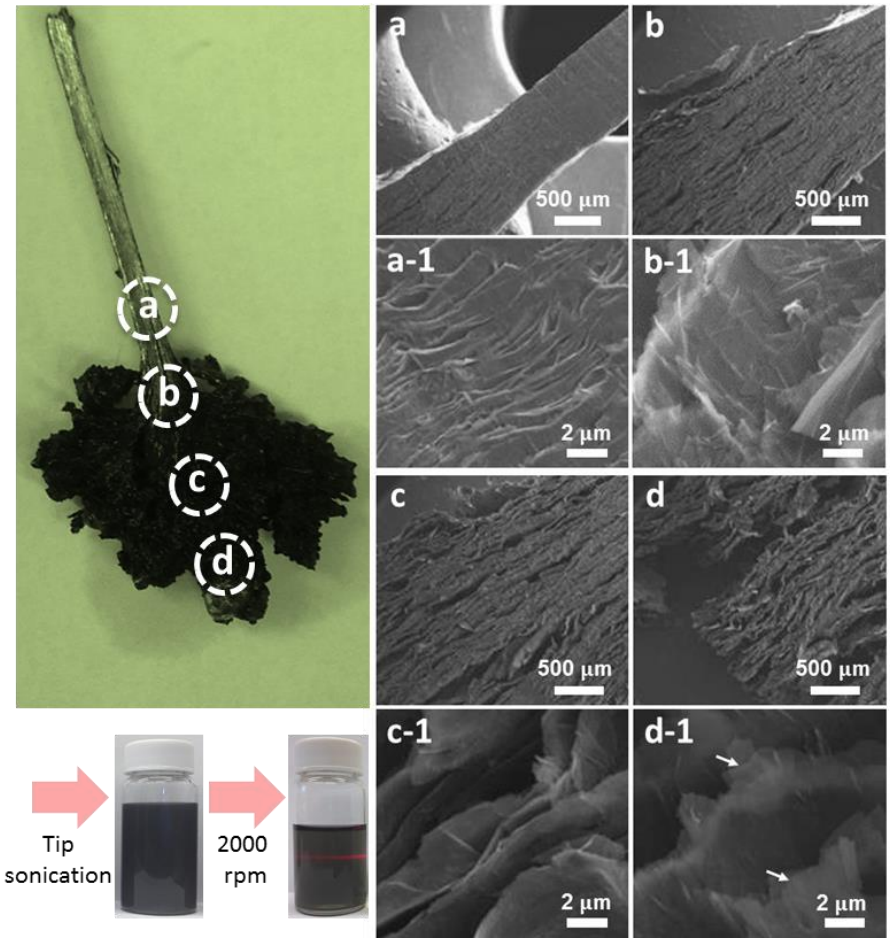

Figure 10. Snapshot and SEM images of electrochemically expanded graphene. Evolution of microstructure from graphite (a) to opened and exfoliated structures of graphene (d). High magnification of upper region of images (a-1), (b-1), (c-1), and (d-1), respectively. Photograph of concentrated graphene dispersion (left) and graphene dispersion (right) after centrifugation in NMP displaying Tyndall effect.

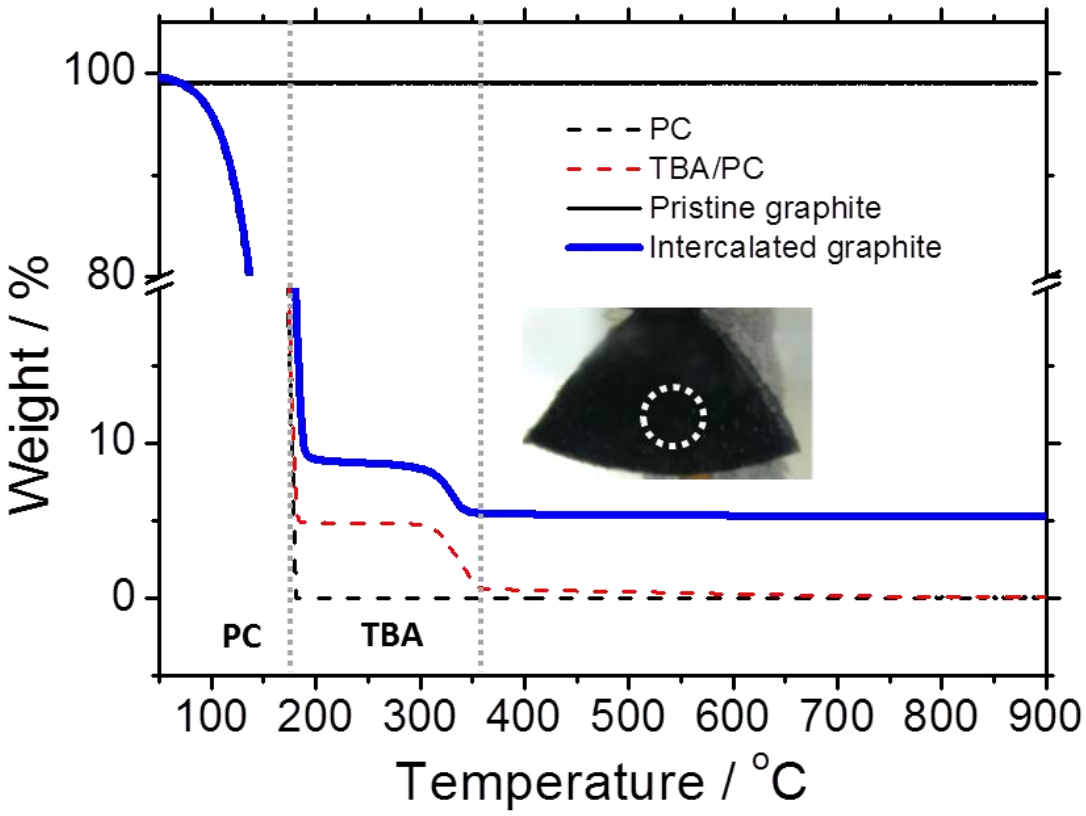

Figure 11. TGA of graphite gasket as a starting material and intercalated graphite after expansion. TGA data for graphite, PC, and TBA^+/PC electrolyte are shown for comparison. The inset figure shows the electrochemical expanded graphite.

Thermogravimetric analysis (TGA) of graphite and graphene were carried out under N_2 flow using TA Instrument thermogravimetric analyzer. The thermal decomposition traces of pure PC and TBA^+/PC in the TGA spectrum are used as references for judging whether the intercalation of PC and TBA^+ occurred or not in the graphite. The samples were heated from 50 to 900℃ at 10℃/min. As expected, graphite was stable up to 900℃ in N_2 gas. TGA of the expanded graphite electrode (Figure 11) revealed a significant amount of intercalation of PC/TBA^+ in the graphite gasket after it expanded. After the full expansion at -2.22 V, we found that intercalated graphite (Figure

11) exhibited up to 95% weight loss in the TGA. The mass of expanded graphene displayed significant decreases from 100 to 200℃ and further mass loses are observed at 350℃. This latter is associated with the thermal decomposition of TBA^+ with PC. These results indicate that a significant amount of PC and TBA^+ are intercalated into graphene sheets and are responsible for the weakened π-π interaction along the c axis. From these studies we can infer that PC/TBA^+ is incorporated as a result of charging voltage being applied. In addition, the graphene prepared here shows a good thermal stability at high temperature, in contrast with graphene oxide, which contains oxygen-containing functional groups and undergoes thermal decomposition to give what is called reduced graphene oxide. [72, 73]

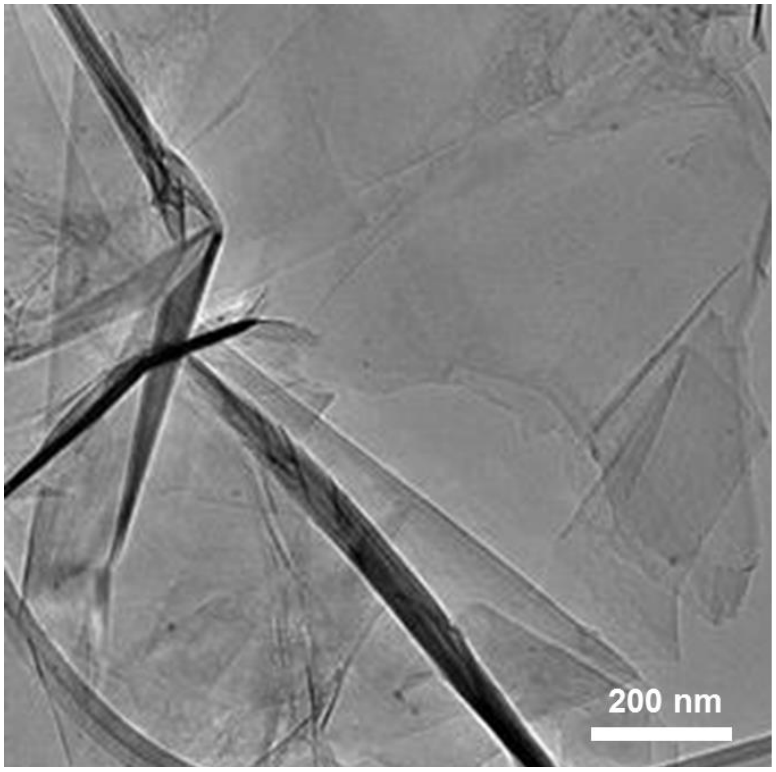

Figure 12. Bright-field TEM images of the few layer graphene produced by the expansion.

We investigated the microstructure of the graphene in the dispersion using transmission electron microscopy (TEM). Samples were prepared by dropping a small quantity of each dispersion onto Lacey carbon grids. For TEM, the expanded graphite was exfoliated via ultrasonic treatment to produce graphene sheets. Graphene in NMP was centrifuged at 2000 rpm and extensively washed (ethanol, ethyl acetate, and acetone). Graphene sheets produced by the electrochemical exfoliation were at most a few layers thick (Figure. 12). As a result of the high surface area of extended thin layers, the graphene sheets have a significant tendency to overlap each sheet and edges of sheets are partially folded due to evaporation of solvent on the grid. This shows that individual sheets of graphene without surface contaminations are present.

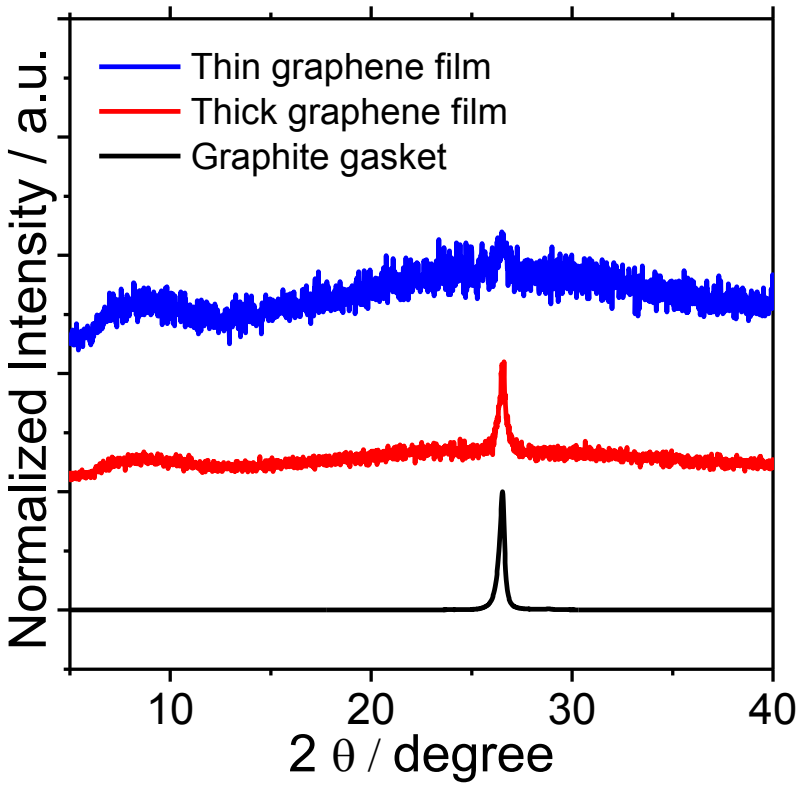

Figure 13. XRD spectra of graphene gasket, thin graphene and thick graphene film on glass.

The graphene were also examined by X-ray diffraction (XRD) patterns to assess whether the long-range periodicity associated with the c axis in thick graphite had been retained in the exfoliated materials. Figure 13 shows XRD patterns of the graphite, and graphene films in Figure 13. The graphite gasket displayed a sharp diffraction peak at 26.5° corresponding to the (002) plane with d-spacing of about 0.335 nm. In contrast, according to the thickness of graphene film, the characteristic peak (002) of the graphene film becomes very weak in intensity and the peak is much broader than that of graphite. The broad peak and the intensity of the graphene film sample confirms an irregular spacing of the graphene.

3.2. Surface Chemical Analysis

3.2.1 X-ray Photoelectron Spectroscopy (XPS)

It is critical to determine the defect level in the exfoliated graphene. The thermal, optical and electronic properties of graphene are extremely sensitive to the presence of defects. To analyze these materials we have applied Raman, infrared, and X-ray photoelectron spectroscopies (XPS). The objective of this study is to evaluate changes in the graphene's chemical state of very thin films composed of graphene as a result of TBA^+ intercalation and electrochemical reactions by using X-ray photoelectron spectroscopy (XPS). Figure 14 shows the XPS survey spectra of the graphite gasket and electrochemically exfoliated graphene over a wide range of binding energies (0-1100 eV). These spectra are dominated by a feature around 283.2 eV, which is associated with graphitic carbons (C 1s) and a weak peak at ~531.2 eV, which is assigned to O 1s.

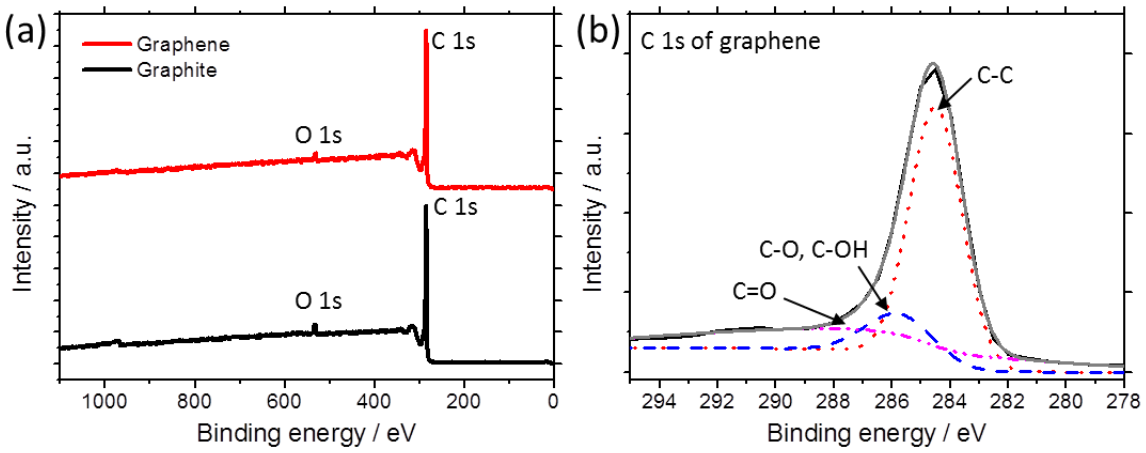

Figure 14. (a) XPS survey scans of graphite and graphene created by electrochemical exfoliation and dispersion in NMP. (b) High resolution spectrum and deconvolution of C 1s XPS spectrum of graphene. The XPS survey spectra recorded in the range of 0-1100 eV.

Although the C 1s XPS spectrum of the exfoliated graphene exhibits these same oxygen functionalities, their peak intensities are much smaller. The oxygen content of the electrochemically exfoliated graphene by using low potential (-2.22 V) is similar to 3 atomic % oxygen content of the graphite gasket which is the starting material (Figure 14a). It is distinct from the previous results that some degree of oxidation of graphene is originated by OH^- ions and oxygenated groups from trapped PC or PC-break decomposition products generated during the electrochemical expansion. [61, 62, 74] In brief, the C 1s XPS spectrum of graphene (Figure. 14) indicates an insignificant degree of oxidation. The C/O ratio of 32.3 for graphene was significantly higher than those reported, indicating that this method provides a higher degree of pristine graphene than the other exfoliated graphenes. [65, 74] In order to fully explain the oxygen functionality in the graphene, the peak at around 283.2 eV was deconvoluted. The deconvoluted XPS spectra

of the C 1s peak (Figure 14b) disclose the presence of sp^2 C-C (~285 eV), C-OH or C-O (~286 eV), C=O (287.6 eV), and a shake-up peak at about 291 eV. [75] From the deconvoluted spectra, the sp^3 C-C content in the sample was very low, confirming that unintended covalent reduction on graphene doesn't occur to a significant extent under our mild conditions. We conclude that electrochemical exfoliation is an effective route to high-quality pristine graphene.

3.2.2 Raman Spectroscopy

Pristine graphenes are known to have limited solution processability, particularly in volatile solvents. Therefore, it is hard to employ conventional coating methods such as drop-casting, spin-coating, and air-brushing. [76-79] To best investigate graphene materials fast and cost effective assembly protocols are crucial after exfoliation.

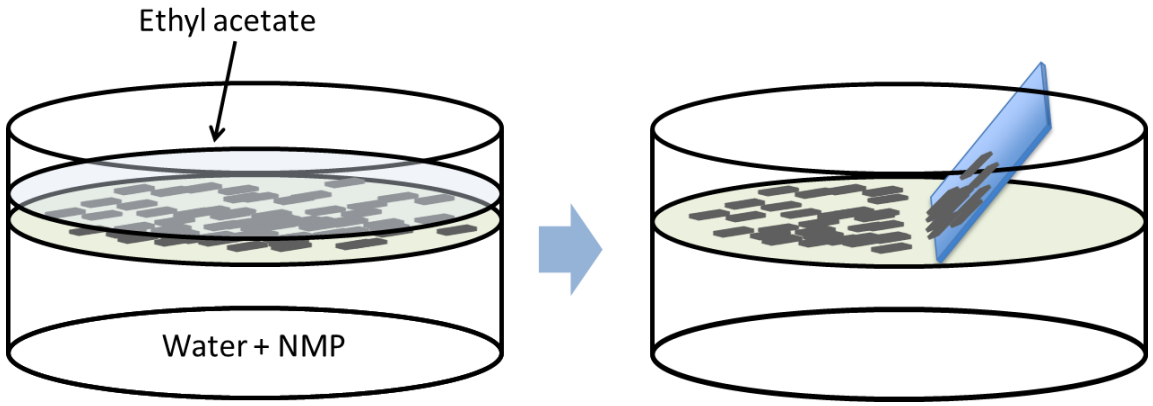

Figure 15. Schematic illustration of graphene assembly and film formation on substrate. Graphene are quickly elevated by Rayleigh-Benard convection and assembled at liquid surface by Marangoni forces.

Shim et al. reported a rapid method for assembling pristine graphene platelets into a large area transparent film at a liquid surface. [80] This assembly principle can be applied to various low dimensional nanomaterials such as graphene, carbon nanotubes and fullerenes. After electrochemical expansion TBA^+-intercalated graphene sheets were suspended in NMP by tip sonication. The graphene remained suspended as a result of the solvation by NMP molecules. To prepare films the graphene suspension is initially dropped into DI water (50%, v/v). Next several drops of ethyl-acetate were immediately introduced to the NMP and water mixture. Graphene then spontaneously assembles into a uniform film on the surface of liquid as illustrated in Figure 15. This process proceeds as Rayleigh-Bénard convection occurs, and the surface tension difference between solvents and Marangoni forces at the interface lead to a graphene film. The graphene films are then transferred from the liquid surface onto a SiO_2/Si substrate for Raman analysis. Figure 16 details the Raman spectrum of the starting graphite, single, and bilayer graphene sheets. These measurements on electrochemically exfoliated graphene films were taken with a 532 nm excitation laser with SiO_2 (300 nm)/Si substrates. The major Raman features of the single layer graphene are G band (~1566 cm^{-1}), D band (~1343 cm^{-1}) and 2D band (~2680 cm^{-1}). The Raman spectra in Figure 16a-b are consistent with single layer graphene displaying a sharp and symmetrical 2D band that can be fit to a Lorentzian/Gaussian function. For single layer graphene the 2D band peak is properly described by a single Lorentzian and 2D band of bilayer graphene is fit with four Lorentzian peaks. The quality of the graphene was monitored by the relative intensity of the defect-related D peak and the G peak (doubly degenerate zone center E_{2g} mode). The D band (~1350 cm^{-1}) gives evidence of the presence of defects, which are caused by the

breathing mode of the sp^2 carbon atoms and activated by the existence of defects such as edges, functional groups, or structural disorder. [81]

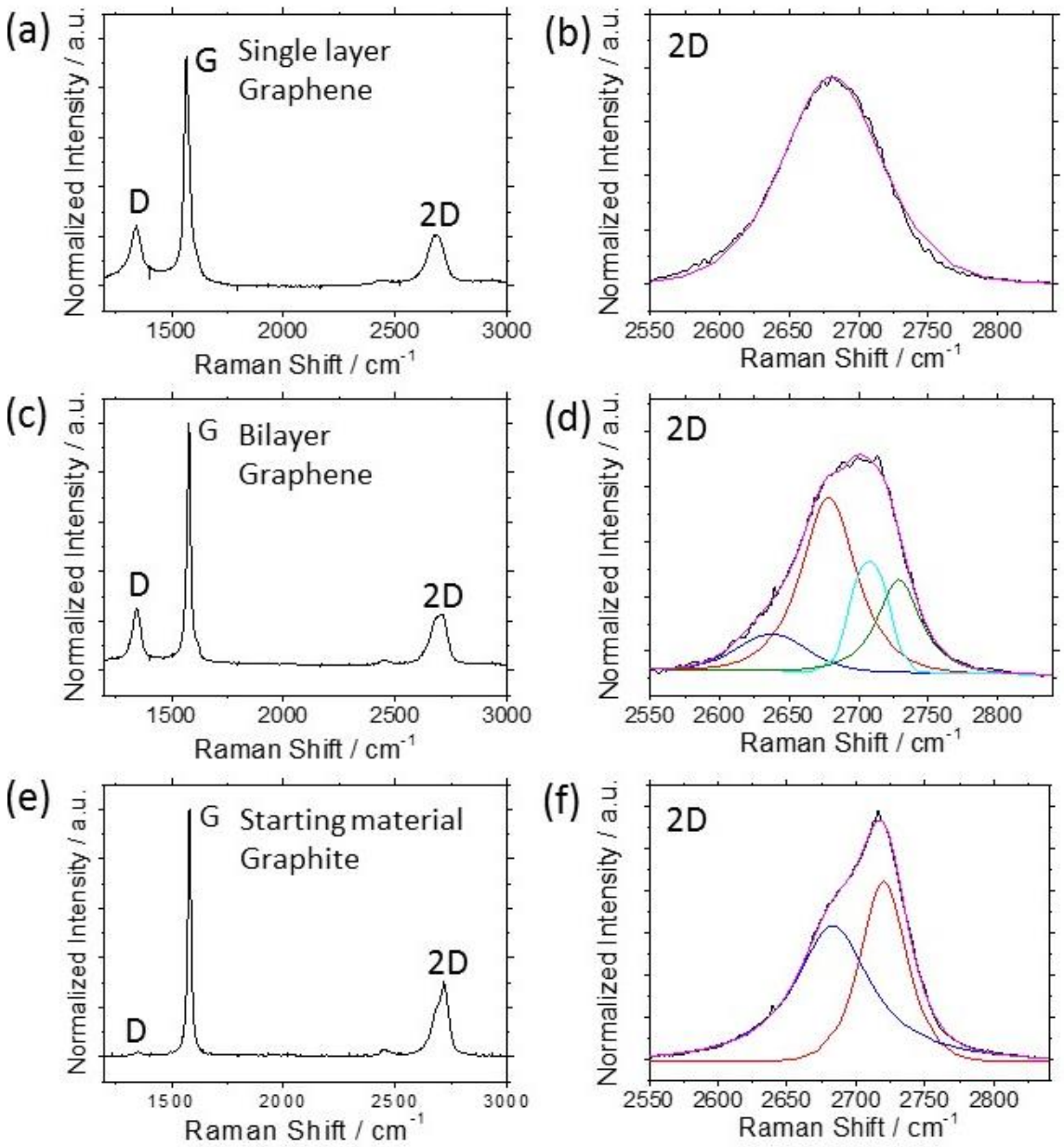

Figure 16. The representative Raman spectra. (Left) Raman spectra (532 nm laser) of graphene on SiO_2/Si substrates compared with the spectrum of graphite; (right) Lorentzian/Gaussian peak fitting of the 2D bands of single, bilayer graphene and graphite.

However, we cannot conclude that some degree of I_D/I_G ratio of the resultant graphene is solely generated from defects in the basal plane of graphene because the size of the resultant graphene plates is less than a micron and edge defects need be taken into account. [82]

The peak intensities of 442 spectra were obtained from the Raman mapping measurement and used to create a histogram of the I_D/I_G ratio (Figure 17). The low intensity D peak intensity (the mean of the I_D/I_G ratio is 0.3) indicates that high quality and low defect graphenes are produced. [83, 84] The I_D/I_G ratio of 0.3 is smaller than that of graphene oxide (> 0.8), chemically reduced graphene oxide (~1.3) and graphene electrochemically exfoliated in acidic solution (~0.4). [65, 85, 86]

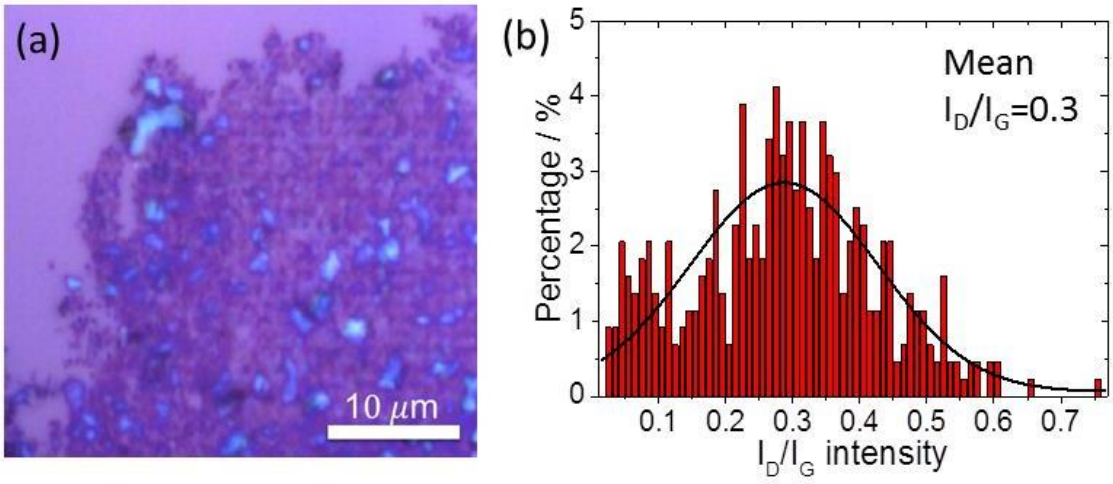

Figure 17. (a) The optical image of graphene film on SiO_2/Si wafer and (b) a histogram of I_D/I_G intensity ratio of electrochemically exfoliated graphene.

On the basis of the Raman peak profile and peak position analysis of the resultant graphenes, we can conclude that > 90% of the bulk material is composed of graphenes with fewer than 5 layers. The sheet resistance of thin films containing only a few layer graphene was measured by the four-point probe technique. When 0.2 mg/cm^2 graphene

was loaded, a sheet resistance was 976 ohm/sq, which is comparable to that of graphene powder. [61] Taken together with the Raman and XPS results, insignificant amounts of oxidation occurs during processing. Thus, we can conclude that the quality of the graphene produced by our method is high, especially when compared to graphene oxide and electrochemically exfoliated graphene performed in acid solution.

3.4 Results and Discussion

A simple and effective solution-based strategy to exfoliate graphene by electrochemical intercalation of graphite gasket materials has been developed. This approach is potentially industrially scalable for the production of conductive low-defect graphene from graphite. It is distinct from the acid-based exfoliation methods (Hummers' method) that produce insulating graphene oxide derivatives. In addition, using a cheap graphite source, this method provides an inexpensive alternative for graphene production as compared to those that begin with HOPG. The intercalated tetrabutylammonium cations are able of expanding the graphite electrode, helping each graphene surface to remain open for further surface chemistry without additional chemical processes. It is necessary to use these methods to broaden the utility of graphene. Our findings enable further investigation of the physical and chemical properties of pristine graphene with few layer structures, and open up a wide spectrum of possibilities for applications including composites, nano-electronics, sensors, and energy technologies. Furthermore, in-situ TEM observation of intercalation processes in graphite is required to study more systematic intercalation mechanisms. In addition, the availability of high-quality,

inexpensive graphenes with accessible surfaces for reactions encourages us to expand solution-based chemical approaches for covalent functionalization.

Chapter 4.

Covalent Diazonium Functionalization of Expanded Graphene

4.1 Introduction

A frequently encountered problem in the functionalization of graphene sheets is their tendency to form irreversible agglomerates or restacking. Covalent modification of graphene surfaces is a leading approach to improving the stability of graphene solutions. Although graphene can be stabilized by non-covalent binding of surfactants or solvent molecules, the covalent approach offers the advantage of permanent stabilization of the isolated graphene sheets. Furthermore, chemical functionalizations that transform graphene carbons from sp^2 to sp^3 can be used to control the electronic properties of graphene by opening band gaps and generating semiconducting regions. [87] These latter features are needed for a number of target applications of graphene. In recent years there has been considerable effort on graphene functionalization. [15, 88] Electrochemical reduction of phenyl diazonium ions on the surface of carbon electrodes was first described by Delamar in 1992, and presently electrografting of organic structures using diazonium chemistry is a recognized method for obtaining functionalized graphene

surfaces. [89, 90] The term electrografting refers to the binding of an organic layer onto a solid conducting substrate. Diazonium ion reduction has several features that make it attractive for surface modification. The electrochemically generated reactive radical is most likely to react with the electrode surface and the electronic changes to the surface create even surface coverage. [91] Additionally, the C-C bond between the phenyl radical and the carbon is stable and has been shown to survive 500℃ in vacuum. [92]

4.2 Electrochemical Diazonium Functionalization on Graphene

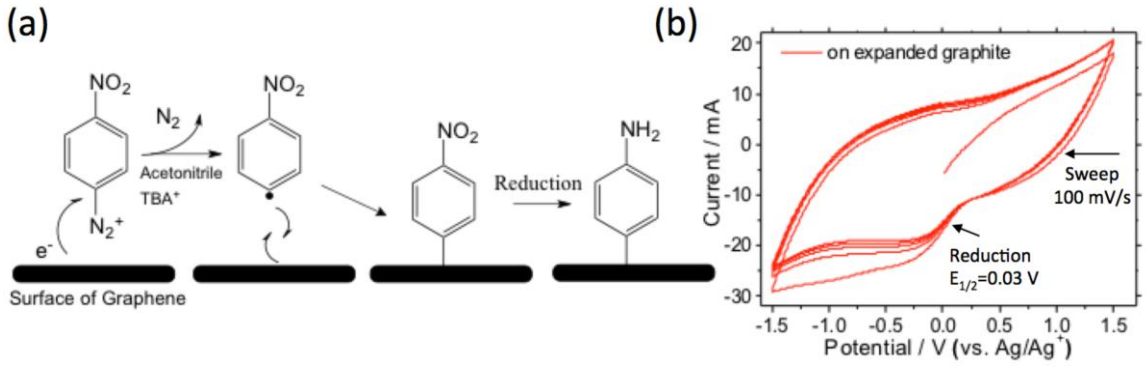

Figure 18. (a) Electrochemical grafting mechanism in the presence of 4-nitrobenzenediazonium (4-NBD) salt on graphene in acetonitrile. The initial reductive activation of graphene enhances the reductive reaction with diazonium ions and the nitrogroups can be further reduced to amines. (b) Cyclic voltammogram of 4-NBD in acetonitrile.

In this chapter we detail diazonium covalent functionalization of the graphene in an electrochemical process. In order to achieve a high yield of surface coverage on bulk graphene the electrochemical route has been chosen. As expected, the delocalized π-electrons of the basal plane of graphene undergo electron transfer reactions with the aryl

diazonium cation, which becomes an aryl radical after releasing N_2 gas. The aryl radical, which is highly reactive, readily forms a covalent bond with a carbon atom in the graphene lattice changing its hybridization to sp^3 as illustrated in Figure 18a [93] Cyclic voltammetry of 4-nitrobenzenediazonium on graphene versus $Ag/AgNO_3$ at 100 mV/s as shown in Figure 18b shows a broad irreversible reduction wave on the first scan that continues to disappear during subsequent scans. This behavior is typical of diazonium salts and the disappearance of the wave corresponds to film formation and passivation of electrode. As will be discussed later, further reduction of the nitro groups can be effected to create pendant amines.

Bulk functionalization was carried out by immersing the expanded graphene in 60 mL of acetonitrile containing 20 mM 4-NBD and 50 mM tetrabutylammonium perchlorate. A constant potential of -0.6 V (vs $Ag/AgNO_3$) was then applied to the expanded graphene for 10 hours without particular care to the dryness of the solvent and with simple bubbling of nitrogen in the solution we obtained electrochemically functionalized graphene. During electrochemical grafting nitrogen bubbles are observed to form on the expanded graphite. After functionalization extensive washing steps were carried out to remove unreacted reagents and non-covalently linked byproducts.

4.3 Results and Discussion

As evidenced by TGA, FTIR, UV-Vis, and XPS analysis (see Figure 19a), covalent functionalization via an electron-transfer reaction with 4-NBD results in nitrobenzene groups being covalently attached to the graphene surface. Significant mass loss was detected when 4-NBD functionalized graphene powder was heated up to 900°C.

After diazonium reduction, the absorption peak of the graphene dispersion at 249 nm shifted to 275 nm as shown in Figure 19c. [94] The presence of NO_2 groups on the graphene surface was also revealed by FTIR spectroscopy (Figure 19c).

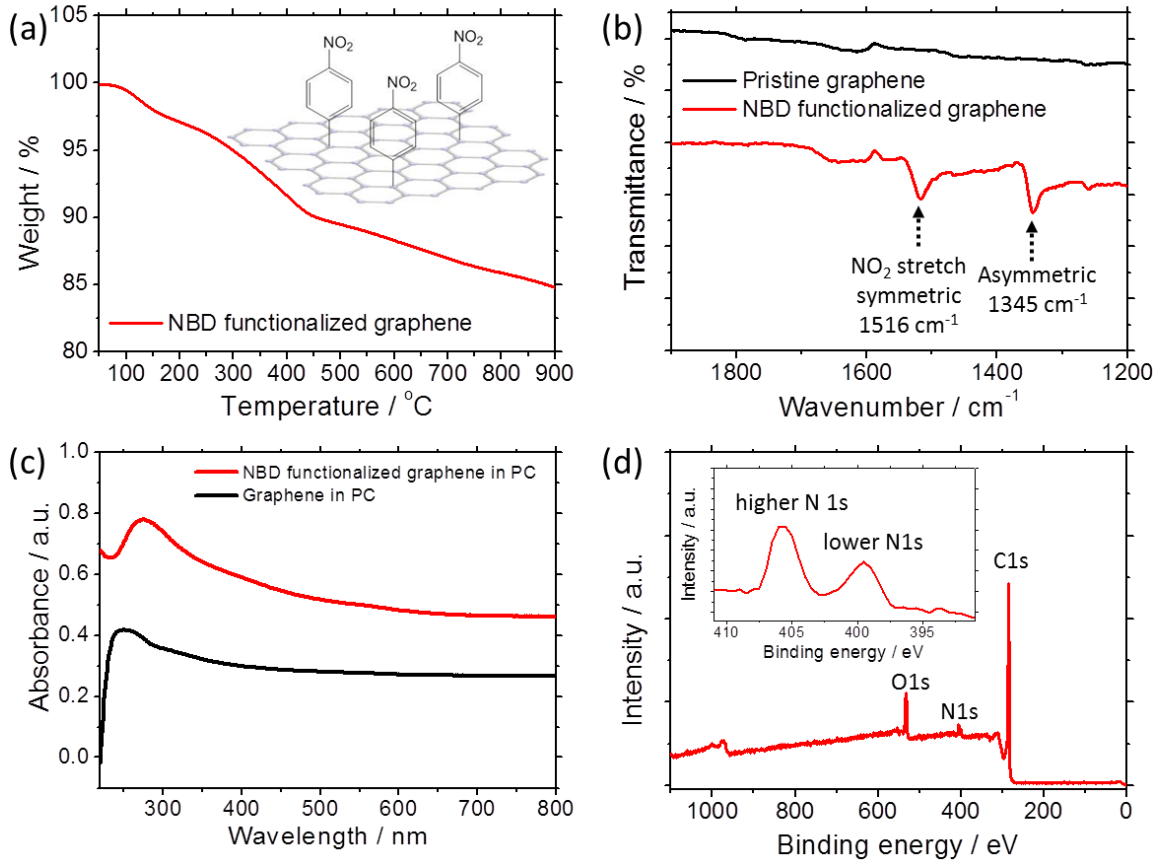

Figure 19. (a) TGA curve, (b) ATR-FTIR spectra of 4-NBD functionalized graphene. (c) UV-Vis absorption spectra of dispersion of graphene and 4-NBD functionalized graphene in propylene carbonate. (d) XPS survey and N 1s high resolution scan of 4-NBD functionalized graphene.

In the FT-IR spectrum of 4-NBD functionalized graphene, the peaks located at ~1516 and 1345 cm^{-1} are attributed to NO_2 symmetric and asymmetric vibrations,

respectively. [87, 89] To probe quantity and the nature of the nitrogen atoms on the functionalized graphene structure, we carried out X-ray photoelectron spectroscopy (XPS). As can be seen in Figure 19d, the XPS survey scan for the 4-NBD functionalized graphene shows a large narrow graphitic C 1s peak at 285 eV, an O 1s peak at 534 eV, and a N 1s peak at 400 eV. At high-resolution the N 1s profile reveals two peaks centered at 399.5 and 405.5 eV (Figure 19d). Both N 1s peaks were observed after extensive washing and filtration of the functionalized graphene with organic solvents and drying the samples in vacuum at 90℃. No nitrogen was found in the untreated pristine graphene, suggesting that the nitrogen content on the graphene originates with nitrobenzene diazonium functionalization. The major peaks are assigned to the nitro group and reduced N species, respectively. The one distinct peak at higher binding energy (405.5 eV) is assigned to the nitro groups and confirms the presence of nitrobenzene groups on the surface of graphene. The broad and lower binding energy N 1s peak at 399.5 eV is associated with the presence of partially reduced nitro groups that are generated electrochemically, and x-ray irradiation may also contribute to transformation of the nitro groups to amine groups in the XPS chamber. [87, 95, 96] XPS was used to estimate the degree of functionalization achieved as 5 atomic % of N 1s and 10 atomic % of O 1s. This coverage ratio of aryl groups on graphene is lower than a previous report (theoretically a close-packed monolayer of vertically oriented nitrobenzene groups represents a coverage of 20~25 N atom %) [87] The residual van der Waals interaction between graphene sheets and the steric hindrance among the aryl groups on graphene may limit the degree of coverage. [97] It is important to note, however, the electrochemical functionalization on expanded graphite is a powerful approach that paves

the way to the preparation of more sophisticated graphene-based chemical structures, and can enable potential applications.

Chapter 5.

Summary

5.1 Summary

As new potential applications of graphene multiply it will become more and more important to be able to produce low defect graphene in large quantities. From the electrochemical experiments conducted in Chapter 2 and 3, we demonstrate a highly efficient electrochemical exfoliation of graphite in organic solvents containing tetraalkylammonium salts that avoid oxidation of graphene and defect generation. The interlayer distance of graphite dramatically increases as a result of the presence of the intercalants. This reduces coupling between graphene layers, changing its volume, and allowing the formation of stable solutions. We also demonstrated the electrochemical functionalization of the expanded graphite with nitrobenzene diazonium salts in Chapter 4. The exact mechanism of the electrochemically driven ion intercalation in graphene is still unclear. Direct experimental approaches using in-situ TEM observation, as well as theoretical modeling, are important methods that could shed light on this process. In addition, to realize the full potential of graphene it is important to consider methods that

can be translated from the laboratory to industrial scale applications that also generate low defect graphene. We believe that the approach outlined in this thesis provides a significant step in that direction.

Reference

1. Geim, A.K. and K.S. Novoselov, *The rise of graphene.* Nature Materials, 2007. **6**(3): p. 183-191.
2. Mayorov, A.S., et al., *Micrometer-Scale Ballistic Transport in Encapsulated Graphene at Room Temperature.* Nano Letters, 2011. **11**(6): p. 2396-2399.
3. Lee, C., et al., *Measurement of the elastic properties and intrinsic strength of monolayer graphene.* Science, 2008. **321**(5887): p. 385-388.
4. Balandin, A.A., *Thermal properties of graphene and nanostructured carbon materials.* Nature Materials, 2011. **10**(8): p. 569-581.
5. Nair, R.R., et al., *Fine structure constant defines visual transparency of graphene.* Science, 2008. **320**(5881): p. 1308-1308.
6. Loh, K.P., et al., *The chemistry of graphene.* Journal of Materials Chemistry, 2010. **20**(12): p. 2277-2289.
7. Novoselov, K.S., et al., *Electric field effect in atomically thin carbon films.* Science, 2004. **306**(5696): p. 666-669.
8. Wallace, P.R., *The Band Theory of Graphite.* Physical Review, 1947. **71**(7): p. 476-476.
9. Castro Neto, A.H., et al., *The electronic properties of graphene.* Reviews of Modern Physics, 2009. **81**(1): p. 109-162.
10. Novoselov, K.S., et al., *Two-dimensional gas of massless Dirac fermions in graphene.* Nature, 2005. **438**(7065): p. 197-200.
11. Craciun, M.F., et al., *Trilayer graphene is a semimetal with a gate-tunable band overlap.* Nature Nanotechnology, 2009. **4**(6): p. 383-388.
12. Mak, K.F., J. Shan, and T.F. Heinz, *Electronic Structure of Few-Layer Graphene: Experimental Demonstration of Strong Dependence on Stacking Sequence.* Physical Review Letters, 2010. **104**(17).
13. Freitag, M., *GRAPHENE Trilayers unravelled.* Nature Physics, 2011. **7**(8): p. 596-597.
14. Rodriguez-Perez, L., M.A. Herranz, and N. Martin, *The chemistry of pristine graphene.* Chemical Communications, 2013. **49**(36): p. 3721-3735.
15. Dreyer, D.R., et al., *The chemistry of graphene oxide.* Chemical Society Reviews, 2010. **39**(1): p. 228-240.
16. Hernandez, Y., et al., *Measurement of Multicomponent Solubility Parameters for Graphene Facilitates Solvent Discovery.* Langmuir, 2010. **26**(5): p. 3208-3213.
17. Georgakilas, V., et al., *Functionalization of Graphene: Covalent and Non-Covalent Approaches, Derivatives and Applications.* Chemical Reviews, 2012. **112**(11): p. 6156-6214.
18. Elias, D.C., et al., *Control of Graphene's Properties by Reversible Hydrogenation: Evidence for Graphane.* Science, 2009. **323**(5914): p. 610-613.
19. Robinson, J.T., et al., *Properties of Fluorinated Graphene Films.* Nano Letters, 2010. **10**(8): p. 3001-3005.
20. Chua, C.K. and M. Pumera, *Covalent chemistry on graphene.* Chemical Society Reviews, 2013. **42**(8): p. 3222-3233.
21. Park, C.H., et al., *Anisotropic behaviours of massless Dirac fermions in graphene under periodic potentials.* Nature Physics, 2008. **4**(3): p. 213-217.

22. Choi, W., et al., *Synthesis of Graphene and Its Applications: A Review.* Critical Reviews in Solid State and Materials Sciences, 2010. **35**(1): p. 52-71.
23. Novoselov, K.S., et al., *A roadmap for graphene.* Nature, 2012. **490**(7419): p. 192-200.
24. Rogers, J.A., T. Someya, and Y.G. Huang, *Materials and Mechanics for Stretchable Electronics.* Science, 2010. **327**(5973): p. 1603-1607.
25. Eda, G., G. Fanchini, and M. Chhowalla, *Large-area ultrathin films of reduced graphene oxide as a transparent and flexible electronic material.* Nature Nanotechnology, 2008. **3**(5): p. 270-274.
26. Kim, K.S., et al., *Large-scale pattern growth of graphene films for stretchable transparent electrodes.* Nature, 2009. **457**(7230): p. 706-710.
27. Lee, S.K., et al., *Stretchable Graphene Transistors with Printed Dielectrics and Gate Electrodes.* Nano Letters, 2011. **11**(11): p. 4642-4646.
28. De Arco, L.G., et al., *Continuous, Highly Flexible, and Transparent Graphene Films by Chemical Vapor Deposition for Organic Photovoltaics.* Acs Nano, 2010. **4**(5): p. 2865-2873.
29. Shao, Y.Y., et al., *Graphene Based Electrochemical Sensors and Biosensors: A Review.* Electroanalysis, 2010. **22**(10): p. 1027-1036.
30. Wu, L., et al., *Highly sensitive graphene biosensors based on surface plasmon resonance.* Optics Express, 2010. **18**(14): p. 14395-14400.
31. Ang, P.K., et al., *Solution-Gated Epitaxial Graphene as pH Sensor.* Journal of the American Chemical Society, 2008. **130**(44): p. 14392-+.
32. Chen, C.W., et al., *Oxygen sensors made by monolayer graphene under room temperature.* Applied Physics Letters, 2011. **99**(24).
33. Wang, Y., et al., *Super-Elastic Graphene Ripples for Flexible Strain Sensors.* Acs Nano, 2011. **5**(5): p. 3645-3650.
34. Schedin, F., et al., *Detection of individual gas molecules adsorbed on graphene.* Nature Materials, 2007. **6**(9): p. 652-655.
35. Arsat, R., et al., *Graphene-like nano-sheets for surface acoustic wave gas sensor applications.* Chemical Physics Letters, 2009. **467**(4-6): p. 344-347.
36. Bae, S.H., et al., *Graphene-based transparent strain sensor.* Carbon, 2013. **51**: p. 236-242.
37. Zhu, Y.W., et al., *Graphene and Graphene Oxide: Synthesis, Properties, and Applications.* Advanced Materials, 2010. **22**(35): p. 3906-3924.
38. Wang, J.T.W., et al., *Low-Temperature Processed Electron Collection Layers of Graphene/TiO2 Nanocomposites in Thin Film Perovskite Solar Cells.* Nano Letters, 2014. **14**(2): p. 724-730.
39. Miao, X.C., et al., *High Efficiency Graphene Solar Cells by Chemical Doping.* Nano Letters, 2012. **12**(6): p. 2745-2750.
40. Wang, Y., et al., *Supercapacitor Devices Based on Graphene Materials.* Journal of Physical Chemistry C, 2009. **113**(30): p. 13103-13107.
41. Si, Y.C. and E.T. Samulski, *Exfoliated Graphene Separated by Platinum Nanoparticles.* Chemistry of Materials, 2008. **20**(21): p. 6792-6797.
42. Kim, T., et al., *Activated Graphene-Based Carbons as Supercapacitor Electrodes with Macro- and Mesopores.* Acs Nano, 2013. **7**(8): p. 6899-6905.
43. Li, X.S., et al., *Large-Area Synthesis of High-Quality and Uniform Graphene Films on Copper Foils.* Science, 2009. **324**(5932): p. 1312-1314.
44. Lee, J.H., et al., *Wafer-Scale Growth of Single-Crystal Monolayer Graphene on Reusable Hydrogen-Terminated Germanium.* Science, 2014. **344**(6181): p. 286-289.
45. Virojanadara, C., et al., *Homogeneous large-area graphene layer growth on 6H-SiC(0001).* Physical Review B, 2008. **78**(24).
46. Hernandez, Y., et al., *High-yield production of graphene by liquid-phase exfoliation of graphite.* Nature Nanotechnology, 2008. **3**(9): p. 563-568.
47. Hummers, W.S. and R.E. Offeman, *Preparation of Graphitic Oxide.* Journal of the American Chemical Society, 1958. **80**(6): p. 1339-1339.
48. Dikin, D.A., et al., *Preparation and characterization of graphene oxide paper.* Nature, 2007. **448**(7152): p. 457-460.
49. Swager, T.M., *Functional Graphene: Top-Down Chemistry of the pi-Surface.* Acs Macro Letters, 2012. **1**(1): p. 3-5.

50. Noel, M. and R. Santhanam, *Electrochemistry of graphite intercalation compounds.* Journal of Power Sources, 1998. **72**(1): p. 53-65.
51. Ogumi, Z. and M. Inaba, *Electrochemical lithium intercalation within carbonaceous materials: Intercalation processes, surface film formation, and lithium diffusion.* Bulletin of the Chemical Society of Japan, 1998. **71**(3): p. 521-534.
52. Armand, M. and P. Touzain, *Graphite Intercalation Compounds as Cathode Materials.* Materials Science and Engineering, 1977. **31**: p. 319-329.
53. Solin, S.A., *The Nature and Structural-Properties of Graphite-Intercalation Compounds.* Advances in Chemical Physics, 1982. **49**: p. 455-532.
54. Novak, P., et al., *Advanced in situ characterization methods applied to carbonaceous materials.* Journal of Power Sources, 2005. **146**(1-2): p. 15-20.
55. Guerard, D. and A. Herold, *Intercalation of Lithium into Graphite and Other Carbons.* Carbon, 1975. **13**(4): p. 337-345.
56. Wagner, M.R., et al., *XRD evidence for the electrochemical formation of Li+(PC)(y)C-n(-) in PC-based electrolytes.* Electrochemistry Communications, 2005. **7**(9): p. 947-952.
57. Chung, G.C., et al., *Origin of graphite exfoliation - An investigation of the important role of solvent cointercalation.* Journal of the Electrochemical Society, 2000. **147**(12): p. 4391-4398.
58. Jeong, S.K., et al., *Interfacial reactions between graphite electrodes and propylene carbonate-based solutions: Electrolyte-concentration dependence of electrochemical lithium intercalation reaction.* Journal of Power Sources, 2008. **175**(1): p. 540-546.
59. Hasegawa, M. and K. Nishidate, *Semiempirical approach to the energetics of interlayer binding in graphite.* Physical Review B, 2004. **70**(20).
60. Spanu, L., S. Sorella, and G. Galli, *Nature and Strength of Interlayer Binding in Graphite.* Physical Review Letters, 2009. **103**(19).
61. Wang, J.Z., et al., *High-Yield Synthesis of Few-Layer Graphene Flakes through Electrochemical Expansion of Graphite in Propylene Carbonate Electrolyte.* Journal of the American Chemical Society, 2011. **133**(23): p. 8888-8891.
62. Zhong, Y.L. and T.M. Swager, *Enhanced Electrochemical Expansion of Graphite for in Situ Electrochemical Functionalization.* Journal of the American Chemical Society, 2012. **134**(43): p. 17896-17899.
63. Cooper, A.J., et al., *Single stage electrochemical exfoliation method for the production of few-layer graphene via intercalation of tetraalkylammonium cations.* Carbon, 2014. **66**: p. 340-350.
64. Su, C.Y., et al., *High-Quality Thin Graphene Films from Fast Electrochemical Exfoliation.* Acs Nano, 2011. **5**(3): p. 2332-2339.
65. Parvez, K., et al., *Electrochemically Exfoliated Graphene as Solution-Processable, Highly Conductive Electrodes for Organic Electronics.* Acs Nano, 2013. **7**(4): p. 3598-3606.
66. Chmiola, J., et al., *Desolvation of ions in subnanometer pores and its effect on capacitance and double-layer theory.* Angewandte Chemie-International Edition, 2008. **47**(18): p. 3392-3395.
67. Rao, B.M.L. and T.R. Halbert, *Supporting Electrolytes Containing Tetrabutylammonium Ions in Li-Tis Cells Intercalation of Tetrabutylammonium Ions in Tis.* Materials Research Bulletin, 1981. **16**(8): p. 919-922.
68. Noel, M. and V. Suryanarayanan, *Role of carbon host lattices in Li-ion intercalation/de-intercalation processes.* Journal of Power Sources, 2002. **111**(2): p. 193-209.
69. Hansen, C.M., *Hansen solubility parameters: a user's handbook*. 2012: CRC press.
70. Chen, X.B., et al., *Interlayer interactions in graphites.* Scientific Reports, 2013. **3**.
71. Sirisaksoontorn, W., et al., *Preparation and Characterization of a Tetrabutylammonium Graphite Intercalation Compound.* Journal of the American Chemical Society, 2011. **133**(32): p. 12436-12438.
72. Choi, E.Y., et al., *Noncovalent functionalization of graphene with end-functional polymers.* Journal of Materials Chemistry, 2010. **20**(10): p. 1907-1912.
73. Stankovich, S., et al., *Synthesis of graphene-based nanosheets via chemical reduction of exfoliated graphite oxide.* Carbon, 2007. **45**(7): p. 1558-1565.
74. Parvez, K., et al., *Exfoliation of Graphite into Graphene in Aqueous Solutions of Inorganic Salts.* Journal of the American Chemical Society, 2014. **136**(16): p. 6083-6091.

75. Webb, M.J., et al., *A simple method to produce almost perfect graphene on highly oriented pyrolytic graphite.* Carbon, 2011. **49**(10): p. 3242-3249.
76. Li, D., et al., *Processable aqueous dispersions of graphene nanosheets.* Nature Nanotechnology, 2008. **3**(2): p. 101-105.
77. Becerril, H.A., et al., *Evaluation of solution-processed reduced graphene oxide films as transparent conductors.* Acs Nano, 2008. **2**(3): p. 463-470.
78. Pham, V.H., et al., *Fast and simple fabrication of a large transparent chemically-converted graphene film by spray-coating.* Carbon, 2010. **48**(7): p. 1945-1951.
79. Wu, Z.S., et al., *Field Emission of Single-Layer Graphene Films Prepared by Electrophoretic Deposition.* Advanced Materials, 2009. **21**(17): p. 1756-+.
80. Shim, J., et al., *Two-Minute Assembly of Pristine Large-Area Graphene Based Films.* Nano Letters, 2014. **14**(3): p. 1388-1393.
81. Chu, P.K. and L.H. Li, *Characterization of amorphous and nanocrystalline carbon films.* Materials Chemistry and Physics, 2006. **96**(2-3): p. 253-277.
82. Khan, U., et al., *High-Concentration Solvent Exfoliation of Graphene.* Small, 2010. **6**(7): p. 864-871.
83. Khan, U., et al., *Size selection of dispersed, exfoliated graphene flakes by controlled centrifugation.* Carbon, 2012. **50**(2): p. 470-475.
84. Paton, K.R., et al., *Scalable production of large quantities of defect-free few-layer graphene by shear exfoliation in liquids.* Nature Materials, 2014. **13**(6): p. 624-630.
85. Eigler, S., C. Dotzer, and A. Hirsch, *Visualization of defect densities in reduced graphene oxide.* Carbon, 2012. **50**(10): p. 3666-3673.
86. Allen, M.J., V.C. Tung, and R.B. Kaner, *Honeycomb Carbon: A Review of Graphene.* Chemical Reviews, 2010. **110**(1): p. 132-145.
87. Bekyarova, E., et al., *Chemical Modification of Epitaxial Graphene: Spontaneous Grafting of Aryl Groups.* Journal of the American Chemical Society, 2009. **131**(4): p. 1336-+.
88. Pinson, J. and F. Podvorica, *Attachment of organic layers to conductive or semiconductive surfaces by reduction of diazonium salts.* Chemical Society Reviews, 2005. **34**(5): p. 429-439.
89. Belanger, D. and J. Pinson, *Electrografting: a powerful method for surface modification.* Chemical Society Reviews, 2011. **40**(7): p. 3995-4048.
90. Delamar, M., et al., *Covalent Modification of Carbon Surfaces by Grafting of Functionalized Aryl Radicals Produced from Electrochemical Reduction of Diazonium Salts.* Journal of the American Chemical Society, 1992. **114**(14): p. 5883-5884.
91. Anariba, F., S.H. DuVall, and R.L. McCreery, *Mono- and multilayer formation by diazonium reduction on carbon surfaces monitored with atomic force microscopy "scratching".* Analytical Chemistry, 2003. **75**(15): p. 3837-3844.
92. Allongue, P., et al., *Covalent modification of carbon surfaces by aryl radicals generated from the electrochemical reduction of diazonium salts.* Journal of the American Chemical Society, 1997. **119**(1): p. 201-207.
93. Jiang, D.E., B.G. Sumpter, and S. Dai, *How do aryl groups attach to a graphene sheet?* Journal of Physical Chemistry B, 2006. **110**(47): p. 23628-23632.
94. Paredes, J.I., et al., *Graphene oxide dispersions in organic solvents.* Langmuir, 2008. **24**(19): p. 10560-10564.
95. Mendes, P., et al., *A novel example of X-ray-radiation-induced chemical reduction of an aromatic nitro-group-containing thin film on SiO2 to an aromatic amine film.* Chemphyschem, 2003. **4**(8): p. 884-889.
96. Sinitskii, A., et al., *Kinetics of Diazonium Functionalization of Chemically Converted Graphene Nanoribbons.* Acs Nano, 2010. **4**(4): p. 1949-1954.
97. Gan, L., D.Y. Zhang, and X.F. Guo, *Electrochemistry: An Efficient Way to Chemically Modify Individual Monolayers of Graphene.* Small, 2012. **8**(9): p. 1326-1330.